

NUMERICAL SIMULATION OF FORCED CONVECTION HEAT  
TRANSFER OF LAMINAR CUO-WATER NANOFLUID FLOW  
THROUGH A HORIZONTAL 180 DEGREE CURVE PIPE

HAMED KHAJEH ARZANI

RESEARCH REPORT SUBMITTED IN PARTIAL FULFILLMENT OF  
THE REQUIREMENT FOR THE DEGREE OF MASTER OF  
ENGINEERING

FACULTY OF ENGINEERING  
UNIVERSITY OF MALAYA  
KUALA LUMPUR

2013

**UNIVERSITI MALAYA**  
**ORIGINAL LITERARY WORK DECLARATION**

Name of Candidate: Hamed Khajeh Arzani

Registration/Matric No: KGY110015

Name of Degree: Master of Mechanical Engineering

Title of Project Paper/Research Report/Dissertation/Thesis ("this Work"):

Numerical simulation of forced convection heat transfer of laminar nanofluid flow  
through a horizontal 180 degree curve pipe

Field of Study: Heat Transfer

I do solemnly and sincerely declare that:

- (1) I am the sole author of this Work;
- (2) This Work is original;
- (3) Any use of any work in which copyright exists was done by way of fair dealing and for permitted purposes and any excerpt or extract from, or reference to or reproduction of any copyright work has been disclosed expressly and sufficiently and the title of the Work and its authorship have been acknowledged in this Work;
- (4) I do not have any actual knowledge nor do I ought reasonably to know that the making of this work constitutes an infringement of any copyright work;
- (5) I hereby assign all and every rights in the copyright to this Work to the University of Malaya ("UM"), who henceforth shall be owner of the copyright in this Work and that any reproduction or use in any form or by any means whatsoever is prohibited without the written consent of UM having been first had and obtained;
- (6) I am fully aware that if in the course of making this Work I have infringed any copyright whether intentionally or otherwise, I may be subject to legal action or any other action as may be determined by UM.

Candidate's Signature

Date

Subscribed and solemnly declared before,

Witness's Signature

Date

Name:

To my parents for their encouragement throughout my education

## **ABSTRACT**

A fluid formed by suspending Nano-scaled metallic or non-metallic particles in base fluids is called a nanofluid. Laminar forced convection heat transfer of the CUO-water nanofluid in a pipe with a return bend is analysed by using a finite volume method. The effects of nanoparticles concentrations and Reynolds number are investigated on the flow and the convective heat transfer behaviour. The results show that the average Nusselt number increases with increasing Reynolds number, and the increment of specific heat in the nanofluid contributes to the heat transfer enhancement. The average Nusselt number in the return bend appears higher than that in the inlet and outlet pipes due to the secondary flows. However, the pressure drop in the pipe largely increases with the increment of nanoparticle volume concentration.

## **ABSTRAK**

Kaedah elemen terbatas digunakan untuk menganalisa pemindahan haba perolakan nanobendalir kuprum oksida secara laminar paksaan di dalam paip yang mempunyai selekoh berbalik. Keputusan menunjukkan bahawa purata nombor Nusselt meningkat dengan bertambahnya nombor-nombor Reynolds dan Prandtl, dan peningkatan haba tentu di dalam nanobendalir menyumbang kepada peningkatan pemindahan haba. Purata nombor Nusselt di dalam selekoh berbalik adalah lebih tinggi berbanding di kedua-dua hujung paip disebabkan aliran sekunder. Namun begitu, perbezaan tekanan di dalam paip bertambah secara langsung dengan pertambahan jumlah isipadu nanopartikel.

## **ACKNOWLEDGEMENTS**

First, I would like to thank my parents for guiding me through my first steps of life and education. I would also like to thank my supervisor, Professor Dr. Saidur Rahman at UM university, who has guided my academic and professional development for the past two years. I would also like to thank my love, my wife, Maryam, who has been supportive of me and my study throughout my graduate educations. And also Thanks My friends Iman and Houman for all the help and support in my study in the Malaysia.

# Table of Contents

ABSTRACT .....	ii
ABSTRAK .....	iii
ACKNOWLEDGEMENTS .....	iv
LIST OF TABLE .....	vi
LIST OF FIGURE.....	vii
Nomenclature .....	ix
Chapter 1 .....	1
1 INTRODUCTION .....	1
1.1 Thermal conductivity augment of nanofluid .....	2
1.2 Nanofluid viscosity.....	3
1.3 Nanofluids convective heat transfer .....	3
1.4 Objective .....	4
Chapter 2.....	5
2 REVIEW OF INTERNAL FLOW AND NANOFLUID CONVECTION LITERATURE .....	5
2.1 Using Nanofluids for Forced Convection Heat Transfer improvement .....	5
2.2 Experimental Investigation of Convective Heat Transfer of water-Nanofluid in a Circular Tube .....	11
2.3 Using a Two Phase Approach to Predict Turbulent Forced Convection of a Nanofluid in a Tube with Uniform Heat Flux .....	12
2.4 Heat Transfer and Hydrodynamic Study of Dispersed Fluids with Submicron Metallic Oxide Particles .....	14
2.5 Investigation on Convective Heat Transfer and Flow Features of Nanofluids .....	16
2.6 Convective Transport in Nanofluids .....	17
2.7 Using water-Nanofluid to improve Heat Transfer for an Electronic Liquid Cooling System.....	19
2.8 Summary of Literature .....	22
3 METHODOLOGY .....	25
3.1 Governing Equations of Fluid Dynamics .....	25
3.1.1 Continuity Equation .....	26
3.1.2 Momentum Equation.....	27
3.1.3 Equation of Energy.....	30
3.2 Finite Volume Method (FVM) .....	33
3.3 Geometric shape and Boundary conditions.....	34
3.4 Validation results.....	38
Chapter 4.....	40
4 RESULTS AND ANALYSIS.....	40
Chapter 5 .....	52
5 CONCLUSION.....	52
References .....	53

## **LIST OF TABLE**

Table 3-1 : Physical properties of water and CUO. ....	36
Table 3-2 : Variations of effective physical properties with concentration. ....	37
Table 3-3 : Boundary conditions in straight pipe. ....	38
Table 3-4 : Nusselt numbers for various Reynolds numbers through pipe. ....	40
Table 4-1 : Variations of inlet velocities (m/s) with Reynolds number and concentration. ....	50

## LIST OF FIGURE

Figure 2-1 : Effect of parameter $\phi$ on fluid temperature profiles.....	7
Figure 2-2 : Influence of $\phi$ on axial growth of fluid mean temperature and wall temperature . .....	8
Figure 2-3 : Effect of $\phi$ on heat transfer coefficient ratio $h_T$ . .....	9
Figure 2-4 : Effect of $\phi$ on wall shear stress rations $\tau_r$ .....	10
Figure 2-5 : Axial values of the turbulent kinetic energy at centerline for water and Cu-water nanofluid. ....	12
Figure 2-6 : Nusselt number along the tube axis.....	13
Figure 2-7 : Heat transfer coefficient versus Reynolds number for titanium oxide-water and alumina-water nanofluids.....	15
Figure 2-8 : Heat transfer coefficient versus velocity in turbulent flow.....	16
Figure 2-9, Continued .....	18
Figure 2-10 : Heat transfer in alumina-water nanofluids: a) $\phi= 0$ b) $\phi= 0.01$ c) $\phi= 0.03$ [27]. .....	19
Figure 2-11 : Mass flow rate and particle concentration impacts on the heat transfer coefficient of the water block [14].....	21
Figure 2-12 : Effect of particle size on hw-block for 6.8% nanoparticle volume concentration. ....	22
Figure 3-1 Control volume for Eulerian approach [28]. ....	26
Figure 3-2 : The numerical algorithm by FVM is shown [33].....	34
Figure 3-3 : Schematic representation for cross section of pipes with return bend. ....	35
Figure 3-4 : Grid sample used in this study .....	35

Figure 3-5 : Boundary conditions for pipes with return bend. ....	36
Figure 3-6 : Use straight pipe and water to comparison numerical with analytic results. ...	38
Figure 3-7 : temperature profiles through straight pipe. ....	39
Figure 3-8 : Nusselt profiles for various Reynolds numbers through pipe. ....	40
Figure 4-1 : Distributions of velocity (A) and temperature (B) of water at $Re=10$ . ....	41
Figure 4-2 : Distributions of velocity (A) and temperature (B) of water at $Re=1000$ . ....	42
Figure 4-3 : shows the path of maximum velocity through the curve. ....	43
Figure 4-4 : Dimensionless velocity and Temperature profiles at various Reynolds numbers at section (A). ....	44
Figure 4-5. Temperature and Dimensionless velocity profiles at various Reynolds numbers at section (B). ....	46
Figure 4-6 : Temperature and Dimensionless velocity profiles at various Reynolds numbers at section (C). ....	47
Figure 4-7 : Comparisons of average Nusselt numbers in various parts. ....	49
Figure 4-8 : Average Nusselt number ratios in entire pipes. ....	50
Figure 4-9 : Dependence of pressure drop on concentration at various Reynolds numbers. ....	51

## Nomenclature

Roman symbols

A define in Eq()

B define in Eq()

$C_D$  drag coefficient

$c_p$  specific heat capacity at constant pressure (J/kg.K)

$d_p$  nanoparticle diameter (m)

$F_d$  drag force (N)

$h$  heat transfer coefficient based on mean temperature (w/m<sup>2</sup>k)

$h_v$  volumetric heat transfer coefficient (w/m<sup>3</sup>k)

$h_p$  liquid-particle heat transfer coefficient (w/m<sup>2</sup>k)

$I$  turbulent intensity

$I_0$  initial turbulent intensity

$k$  turbulence kinetic energy (m<sup>2</sup>/s<sup>2</sup>)

$n$  empirical shape factor

$Nu$  Nusselt number ( $h.D/k$ )

$Nu_p$  particle Nusselt number

$p$  static pressure (N/m<sup>2</sup>)

$Pr$  liquid Prandtl number

$q''$  heat flux (w/m<sup>2</sup>)

$Re$  Reynolds number ( $\frac{\rho v_{in} D}{\mu}$ )

$Re_p$  Reynolds number  $(\frac{\varphi_l \rho_l |\vec{V}_l - \vec{V}_p| d_p}{\mu_l})$

$r, z$  2-D axisymmetric coordinates (m)

$S$  rate of deformation ( $s^{-1}$ )

$T$  temperature (K)

$T'$  fluctuating part of temperature (K)

$v$  velocity (m/s)

$v'$  fluctuating part of velocity (m/s)

#### Greek letters

$\varepsilon$  dissipation rate of turbulence kinetic energy ( $m^2/s^3$ )

$\mu$  dynamic viscosity (kg/m s)

$\mu_t$  turbulent viscosity (kg/m s)

$\rho$  density ( $kg/m^3$ )

$\tau$  shear stress (Pa)

$\tau^T$  Reynolds stress (pa)

$\beta$  friction coefficient ( $kg\ m^{-3}s^{-1}$ )

$\kappa$  thermal conductivity (W/m K)

$\Gamma$  define in Eq()

$\omega$  define in Eq()

$\nu$  kinematic viscosity

$\varphi$  particle volume fraction

$\psi$  sphericity

## Subscriptions

eff effective

f fluid

p particle phase

r radial direction

s solid

w wall

z axial direction

- mean

0 initial

# Chapter 1

## 1 INTRODUCTION

Recently almost all advances and developments in industrial technology are being focused on the reduction of system processes leading to higher power concentrations for a wide range of applications. Consequently the need to increase in cooling capacities has been vital for these compact thermal systems. The conventional methods for example using extension surfaces like fins or utilizing micro channels with high heat transfer surface availability to obtain this prompted cooling efficiency have been extensively employed and are restricted in effectiveness. On the other hand, the cooling fluid characteristics, have been investigated recently.

Due to low conductivity characteristic of fluids, they do not have the enough capability to be used in high heat transfer efficiency equipment. In other words, fluids with characteristically poor heat transfer in one hand and increasing needs to micro-scale thermal systems in today's world on the other, have forced the researchers to find the new techniques of heat transfer enhancement. Inevitably one possible solution to overcome this restriction can be obtained by the high heat transfer ability of solid metal particles which are suspended inside flowing fluid. Previously there have been some efforts to add micro-scale metal particles into conventional fluids. Although this way could cause some remarkable outcomes it led to significant shortcomings. These micro-particles, could enhance the heat transfer

characteristic of fluid while impose some negative effect such as increase of viscosity resulting in the need to a more pumping power.

Nanofluid is defined as a new kind of fluid with metallic nanoparticles suspension among liquid molecules. Heat transport of nanofluid is a function of dimension, properties and solid volume concentration of nano-particles. According to experimental investigations nanofluids have shown a significant potential for augmentation of energy transfer and also enormously higher thermal conductivities in comparison to base fluids. Owing to the nanofluids characteristics, many kinds of industries including automotive radiator systems, computer processing cooling equipment, home heating and cooling appliances, power plant cooling systems can utilize from this technique.

The application of high conductivity heat transfer fluids will bring about entirely using the accessible energy of a system which will associate the reduction of negative environmental impacts of companies as well as their operating costs.

One of advantages for nanoparticles is that these nano-particles have great surface area for thermal conductivity than pure fluids [1, 2].

### **1.1 Thermal conductivity augment of nanofluid**

The fast progress trend in manufacturing methods and nanotechnology, the production of nanoparticles (particle size less than 100 nm) has been possible [3]. The first and most important property of nanofluid is the enhanced effective thermal conductivity with addition a small fraction of nanoparticle to base fluid [3, 4]. Since then, roughly all investigation results have shown numerous improvements by use of nanoparticles as additives to enhance heat transfer of fluids and their thermal performance [5-7].

## **1.2 Nanofluid viscosity**

Since the nanofluid convective heat transfer performance is a function of both thermal conductivity and viscosity, it is important to study nanofluid viscosity employing by a system[8]. The viscosity of a fluid is expected to increase as particles are added, no matter if the particles are rotating or non-rotating in the flow field [9]. In this case study, the laminar regime, the pressure drop along a tube is tied to viscosity. This raise of viscosity will result in an unwanted increase in pumping power [10].

## **1.3 Nanofluids convective heat transfer**

Since nanofluid technique has shown the high potential especially in micro and mini-scale devices, a wide range of attentions has been paid to convective heat transfer improvement by this method during recent decades.

However, There are inconsistent results in case of convective heat transfer coefficient or Nusselt number for nanofluids [11]. Similar to conventional base fluid, Nusselt number increases as Reynolds number due to strengthen turbulent mechanism. Identically the particle volume fraction increase leads to raise of heat transfer. In particular, the ratio of Nusselt number is varied from 1.06 to 1.39 for copper-water nanofluid, while the volume fraction of copper particles increased from 0.5% to 2% at the same constant Reynolds number [11, 12]. Moreover, the results depict that prediction of Nusselt number can be failed for nanoparticle volume concentration much more than 0.5% [13]. Accordingly, the energy exchange enhancement rate may be caused by the random movement of nanoparticles. The particle random movements not increases only slip velocity between the fluid and the particles but it is also caused to increase the temperature gradient between the fluid and the tube wall. In

pressure drop point of view experimental findings pronounced that the nanofluids friction factors behaviour is like their base fluids. There are also several studies based on nanofluids in the turbulent flow regime under various kinds of nanoparticle materials, base fluid materials, different fluid mixtures and flow rate combinations. Totally owing to the research outcomes, it is concluded that, the rate of heat transfer enhancement of nanofluids increases while the Reynolds number and volume concentration of particles raise. However, it should be considered that the augmentation magnitudes were not consistent [12, 14-18]

This research is aim to assess thermal and hydrodynamic nanofluid behaviour of laminar forced convection in horizontal pipe with return bend by Computational Fluid Dynamic (CFD) Simulation.

#### **1.4 Objective**

- To carry out background/literature study in thermal and hydrodynamic nanofluid behaviour of laminar forced convection in horizontal pipe with return bend by Computational Fluid Dynamic (CFD) Simulation.
- To investigate the heat transfer in the return bend, inlet and outlet pipes due to the secondary flows because of the centrifugal force.
- To analyse the effects of particle volume fractions and Reynolds number in range of laminar flow on heat transfer.
- Using CFD to predict the pressure drop in the return bend, inlet and outlet pipes.

# Chapter 2

## 2 REVIEW OF INTERNAL FLOW AND NANOFLUID CONVECTION LITERATURE

### 2.1 Using Nanofluids for Forced Convection Heat Transfer improvement

There are an extensive range of studies pronouncing the conductivity improvement of fluid by addition of nanoparticles to fluids. In these studies the nanofluid conductivity improvements have been justified based on several hypothesis such as: surface roughness effect, chaotic movement known as Brownian motion and particle-particle interactions of suspended nanoparticles, high specific area which increases heat transfer surface between fluids and particles, and particle clustering which creates high-conductivity heat transfer paths.

In an effort to reduce the experimental artefact caused by the traditional “hot-wire” approach to measure nanofluid thermal conductivity, some groups selected optical measurement methods, and did not obtain great augmentations in the effective thermal conductivity [19-21]. Putnam et al. [19] concluded the independency of effective static thermal conductivities of gold nanofluids from measure of particle. The thermal conductivity of Au and alumina oxide ( $\text{Al}_2\text{O}_3$ ) nanofluids was calculated by Venerus et al. [20] during forced Rayleigh scattering measurement technique. The thermal conductivity has been obtained by their measurements shows temperature independency while the augmentations

were reliable according to the predictions of the classical effective conductivity theorem. Also, measurements on monodisperse polymer suspensions by Rusconi et al. [21] did not represent a numerous increase in thermal conductivity, but rather followed the classical models for the effective properties of composite media.

Maiga, Palm, Nguyen et. al. [22] simulated laminar forced convection in a pipe with uniformly heated-wall. They adopted alumina particles suspending in water as well as ethylene glycol. They proposed that both heat transfer coefficient and wall shear stress increase as nanoparticle volume concentration and Reynolds number increases. They also achieved that although heat transfer enhancement was more significant in the ethylene glycol mixture than in the water mixture, the ethylene glycol made more unsuitable influences on the wall shear stress. All of the results presented are for a water/alumina mixture with a Reynolds number of 500 and a wall heat flux of 10,000 W/m<sup>2</sup>, but the same behaviours were found in the ethylene glycol mixture.

Figure 2-1 illustrates the effect of particle volume concentration on the radial temperature distribution.

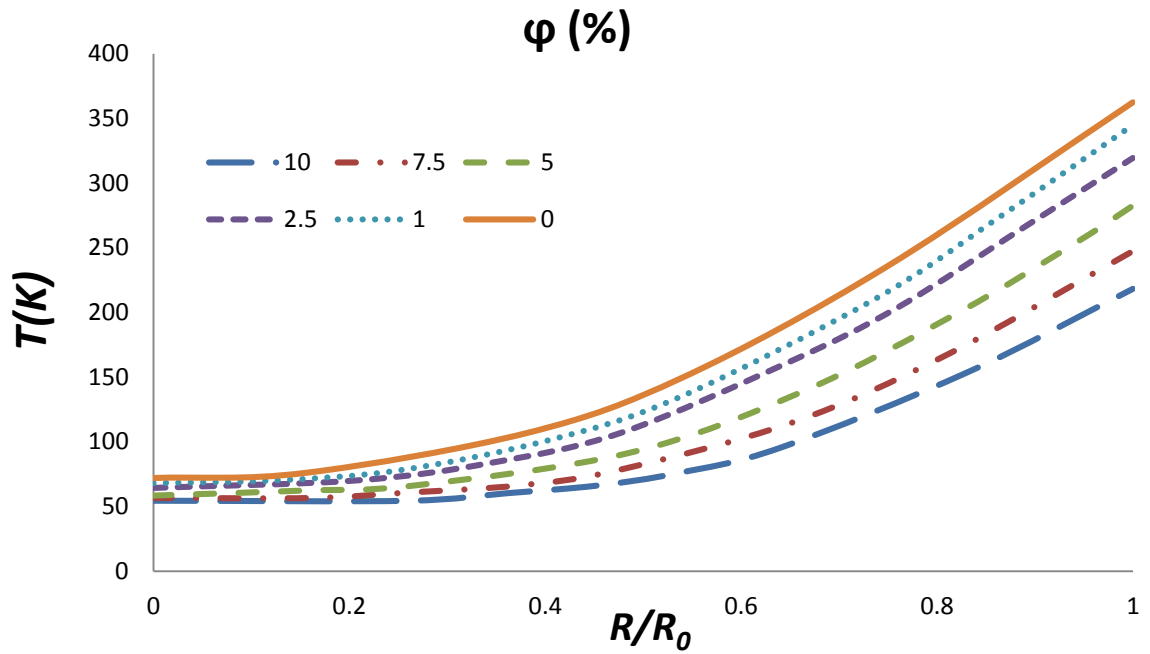


Figure 2-1 : Effect of parameter concentration ( $\phi$ ) on fluid temperature profiles [22].

Figure 2-1, the fluid temperatures decrease with an increase of  $\phi$ , especially near the wall where  $R/R_0=0$ , pronounces higher heat transfer rate in presence of nanoparticles. Accordingly Maiga et. al. found that the wall temperature of the pipe depends on nanoparticle volume fraction more severely than the base fluid temperature, in itself, leads to more heat elimination near the wall of the pipe.

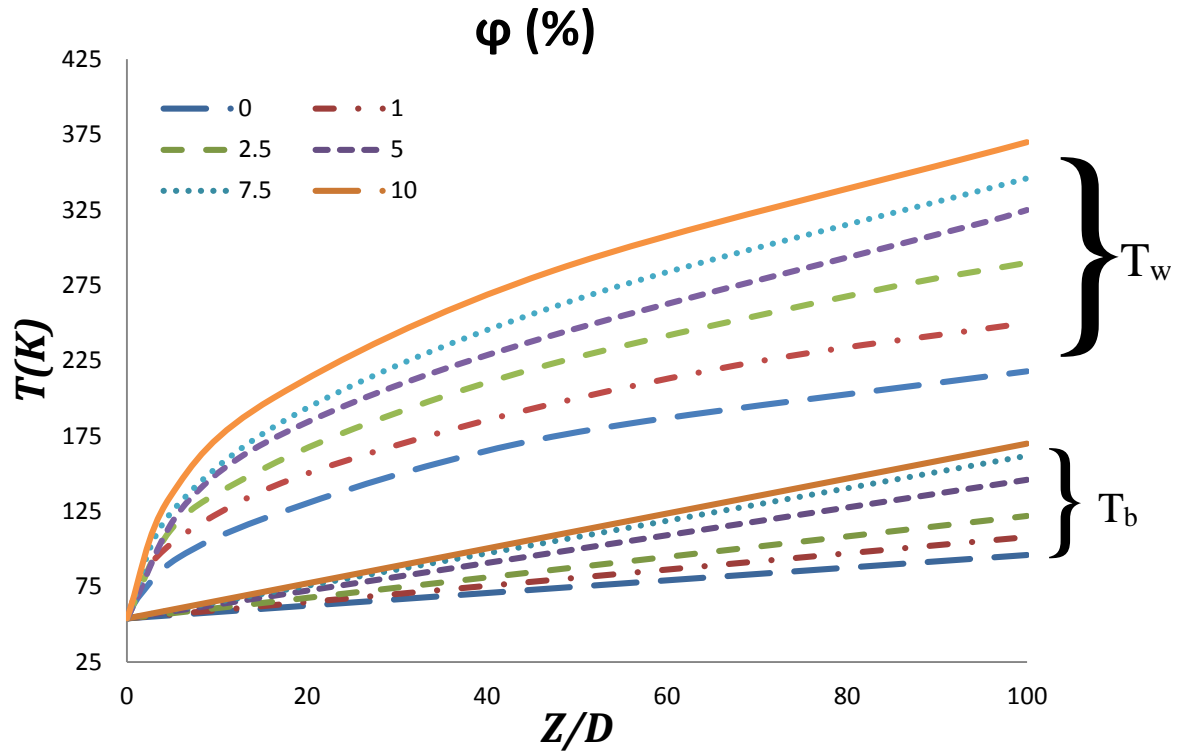


Figure 2-2 : Influence of  $\phi$  on axial growth of fluid mean temperature and wall temperature [22].

Moreover, it can be seen that the decrease in fluid temperature does not take place along the entire length of the tube, and the largest decrease occurs at the tube exit. Due to

Figure 2-1 and Figure 2-2, adding nanoparticles to the fluid causes an apparent heat transfer augmentation. Figure 2-3 depicts the heat transfer coefficient versus the position within pipe length.

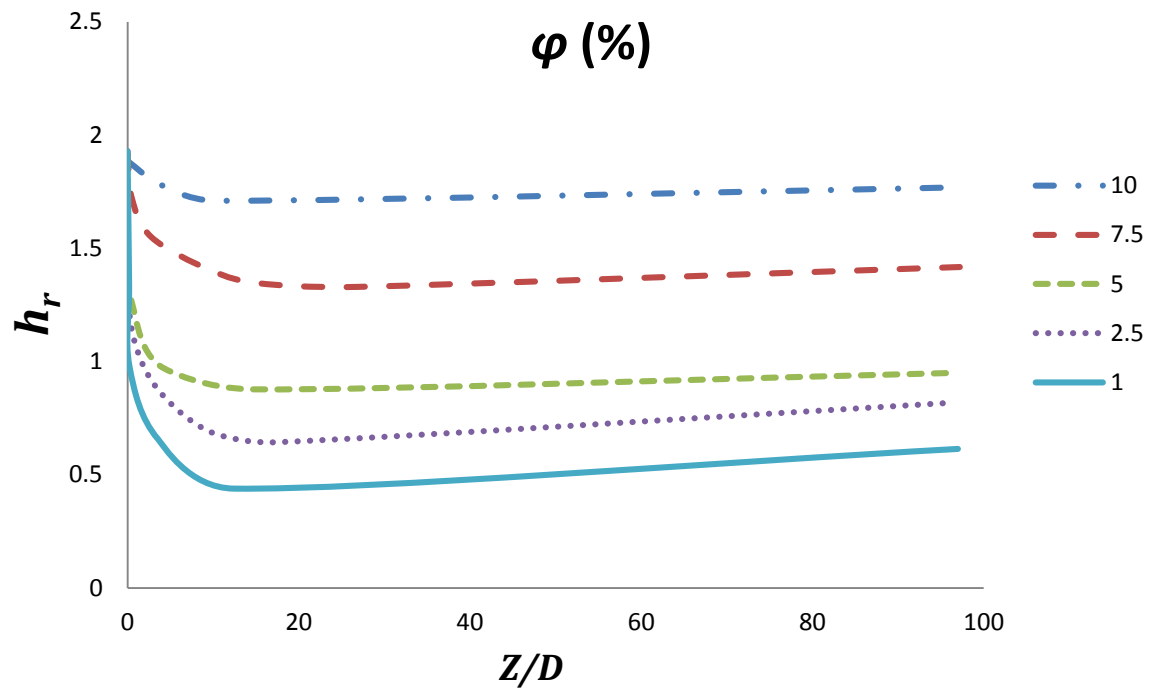


Figure 2-3 : Effect of  $\phi$  on heat transfer coefficient ratio  $h_T$  [22].

At the first glance, Figure 2-3 shows that the heat transfer coefficient increases significantly, while it reaches as much as 63% higher than the heat transfer coefficient of the base fluid at least. Apparently, the heat transfer ratio raises with increasing in nanoparticle volume fraction. As closing to the end of the pipe, the heat transfer ratio goes up, except for the lower nanoparticle volume concentrations which increases with less slope. On the other hand, Figure 2-4 shows the effect of the nanoparticle volume fraction on the wall shear stress.

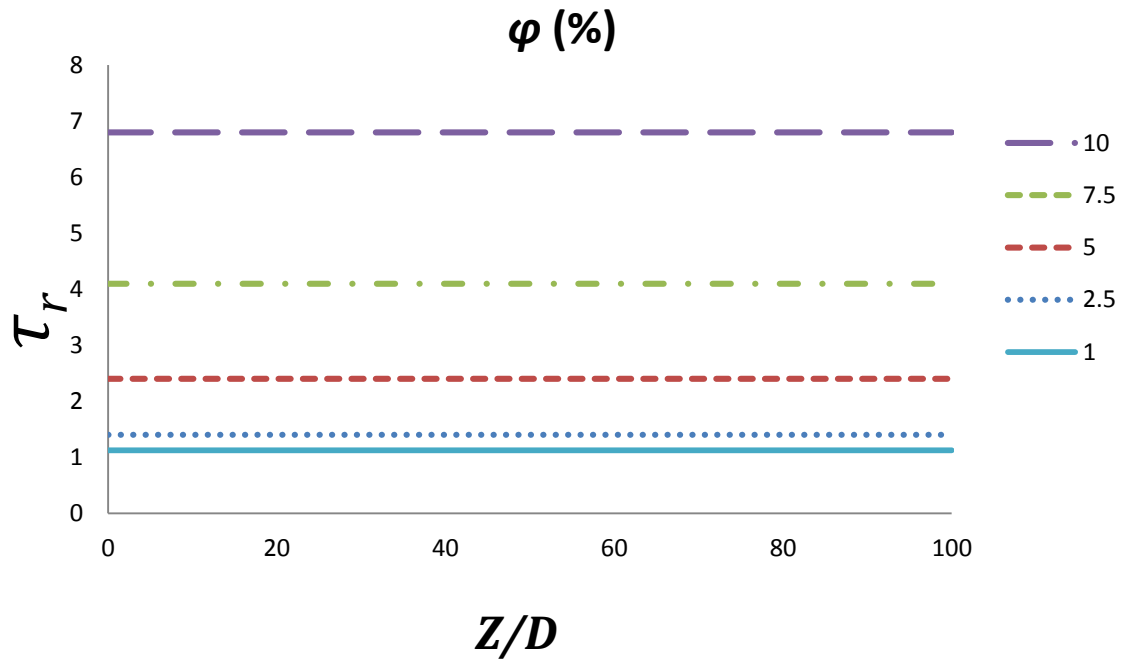


Figure 2-4 : Effect of  $\phi$  on wall shear stress ratios  $\tau_r$  [22]

It is observed that the wall shear stress ratio leftovers constant along the pipe length while it increases with nanoparticle volume fraction.

Maiga, et. al. [22] simulated laminar forced convection inside a pipe. The increase in both heat transfer coefficient and wall shear stress reported as nanoparticle volume concentration increases. Ethylene glycol showed ability to eliminate more heat, although it caused increase in wall shear stress. However, their study was not involved calculation of optimum nanoparticle volume concentration for heat transfer. Most likely, at a specific point adding more nanoparticles leads to adverse effects on heat transfer.

## 2.2 Experimental Investigation of Convective Heat Transfer of water-Nanofluid in a Circular Tube

Heris, Esfahany, and Etemad [23] completed a similar study to Maiga, Palm, Nguyen, et. al except that it includes experimental results as opposed to numerical results. They analyzed laminar forced convection of alumina-water nanofluid inside a pipe with a constant wall temperature. They also reported that the heat transfer coefficient increases as the concentration of nanoparticles increases. Heris, Esfahany, and Etemad showed all of their results versus Peclet number to relate advection and diffusion rate given in Eq. [23]

$$Pe = RePr = \frac{\bar{U}D}{\alpha} \quad (2.1)$$

where Pe is the Peclet number, Re is the Reynolds number, Pr is the Prandtl number, U is the free stream velocity, D is the Diameter of the tube, and  $\alpha$  is the thermal diffusivity.

The theoretical results compared to the experimental results according Seider-Tate correlation, only takes into account an increase in thermal conductivity as a mechanism of heat transfer enhancement. Almost all the experimental results show the heat transfer coefficient of nanofluids higher than that of theoretical. Additionally, the experimental results all have reported higher the heat transfer coefficient than that of base fluid. Since the Seider-Tate equation only considers thermal conductivity increase, which is of a heat transfer coefficient lower than the experimental one, it can be concluded existing more mechanisms for heat transfer enhancement, such as nanoparticle clustering, nano convection, and other dynamic conditions.

### 2.3 Using a Two Phase Approach to Predict Turbulent Forced Convection of a Nanofluid in a Tube with Uniform Heat Flux

The turbulent forced convection heat transfer in a pipe with 1% volume concentration of Cu-water nanofluid Behzadmehr, was studied by Saffar-Avval, and Galanis [24] numerically. They employed the numerical two-phase approach, meaning that the nanoparticles are supposed to have the different velocity from the fluid. In this study,  $Z$  is the tube length,  $D$  is the pipe diameter,  $k_c$  is the turbulent kinetic energy, and  $Nu$  is the Nusselt number. Figure 2-5 illustrates the turbulent kinetic energy at the centreline of pipe versus the dimensionless position along the pipe length.

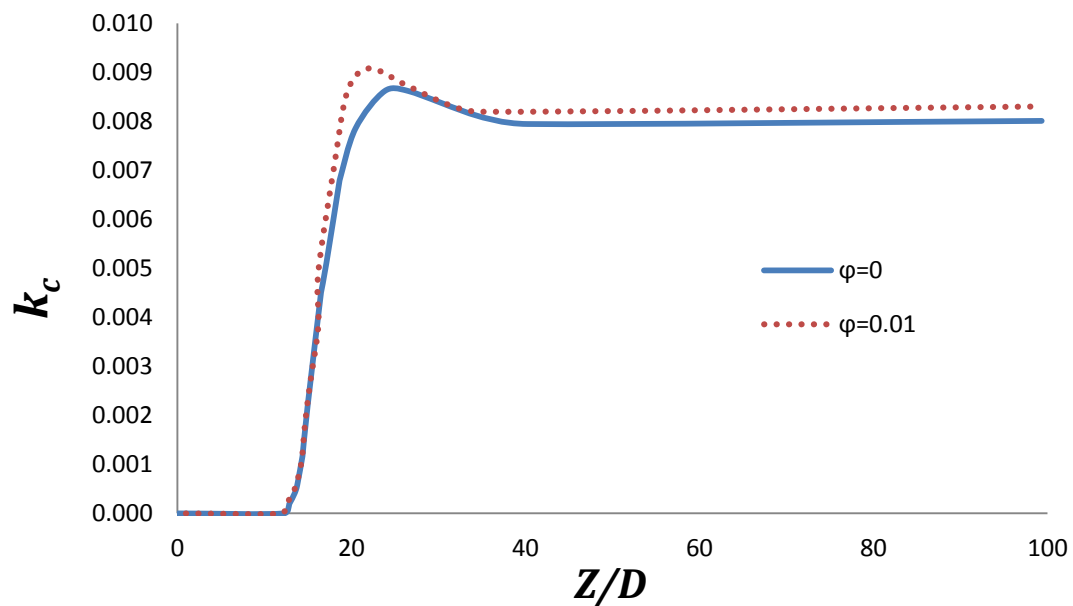


Figure 2-5 : Axial values of the turbulent kinetic energy at centreline for water and Cu-water nanofluid [24].

Due to Figure 2-5 the turbulence flow meet fully developed requirement at  $Z/D=50$ . On the other hand, the kinetic energy increases rapidly to reach the maximum point where the diffusing turbulence touches hits centreline. Figure 2-5, also shows that the nanofluid is of lower values of turbulent kinetic energy than the water. This means that some of the energy of the velocity and fluctuations are absorbed by nanoparticles. This pattern is followed for higher particle concentrations. Additionally as particle concentrations increase, the turbulent kinetic energy decreases. Behzadmehr, Saffar-Avval, and Galanis also draw comparison among different Nusselt numbers corresponding to different Reynolds numbers versus the position along the pipe length, which is shown in Figure 2-6.

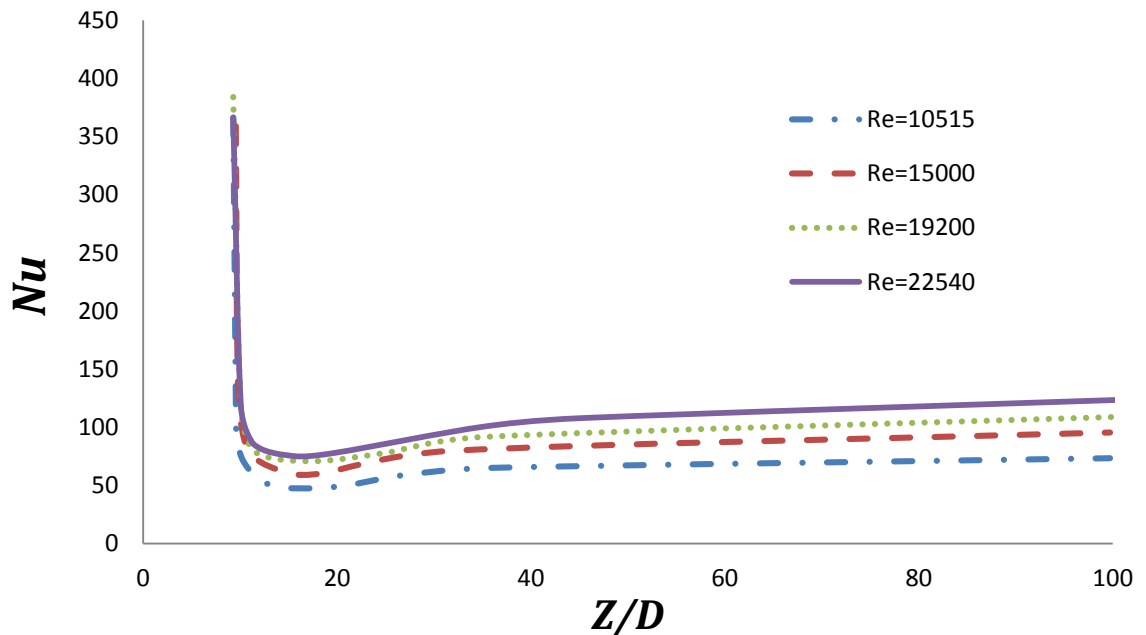


Figure 2-6 : Nusselt number along the tube axis [24].

Due to Figure 2-6, it can be concluded that the increasing Reynolds number leads to the Nusselt number and consequently the heat transfer coefficient increases.

As a result, Behzadmehr, Saffar-Avval, and Galanis [24] reported that adding nanoparticles in turbulent forced convection is effective in augmenting the heat transfer abilities of the base fluid because nanoparticles can reduce the turbulent kinetic energy by absorption of the velocity fluctuation energy .

#### **2.4 Heat Transfer and Hydrodynamic Study of Dispersed Fluids with Submicron Metallic Oxide Particles**

Pak and Cho [25] studied friction and heat transfer of turbulent nanofluid flows in a pipe experimentally. They did the experiment based on alumina and titanium oxide nanoparticles with mean diameters of 13 and 27 nm, respectively, in water. They reported that putting a 10% volume concentration of alumina in water raised the fluid viscosity 200 times while putting the same volume concentration of titanium oxide added a viscosity 3 times greater than water. They also concluded that the nanofluids friction was adapted closely with the Kays correlation for turbulent flow. They draw comparison the heat transfer coefficient versus Reynolds number as be illustrated in Figure 2-7.

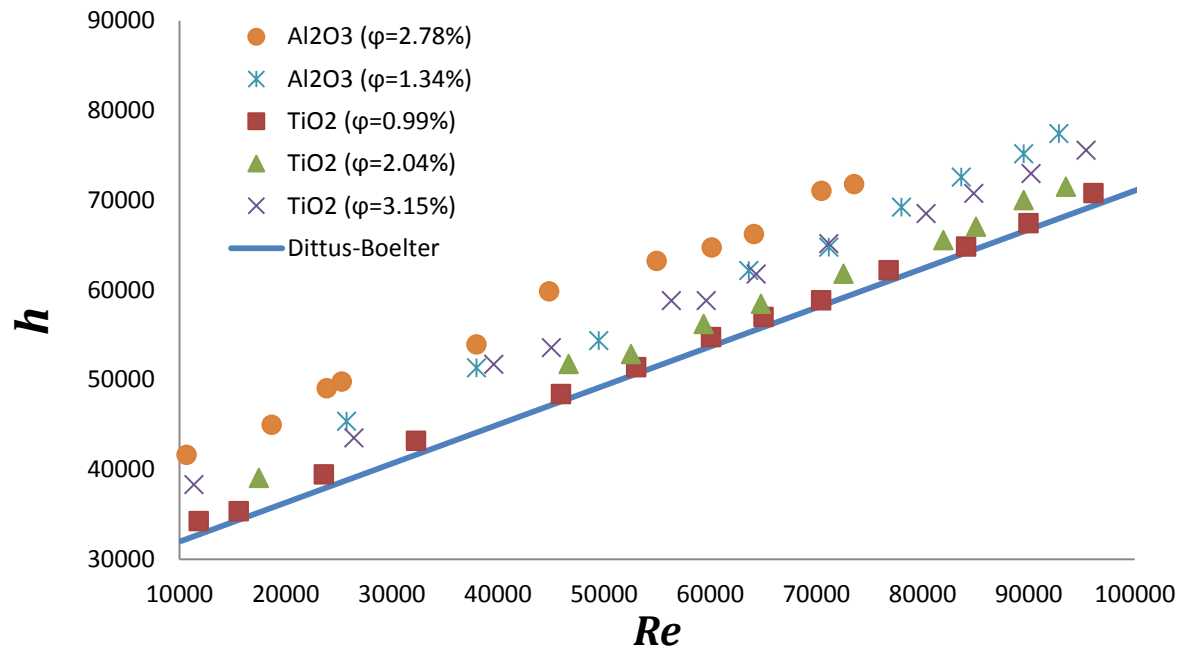


Figure 2-7 : Heat transfer coefficient versus Reynolds number for titanium oxide-water and alumina-water nanofluids [25].

According Figure 2-7, the heat transfer coefficient increases from 45% to 75%, while volume concentration of alumina raises from 1.34% to 2.78%. The alumina nanofluid is consistently higher than the titanium oxide nanofluid. Pak and Cho considered this results due to “enhanced mixing are brought about by submicron particles near the walls”. They plotted the Nusselt number versus the Reynolds number, and observed the Nusselt numbers follow the trend similar to heat transfer coefficient in Figure 2-7.

## 2.5 Investigation on Convective Heat Transfer and Flow Features of Nanofluids

Xuan and Li [11, 26] carried out an experimental investigation on turbulent convective heat transfer of nanofluids in a tube. They assessed the effect of volume fraction and Reynolds number. Copper powders in scale of below 100 nm in diameter were added to water, while the nanoparticle concentration was changed from 0.3% to 2.0%. The heat transfer coefficient calculated from their experiment is shown in Figure 2-8.

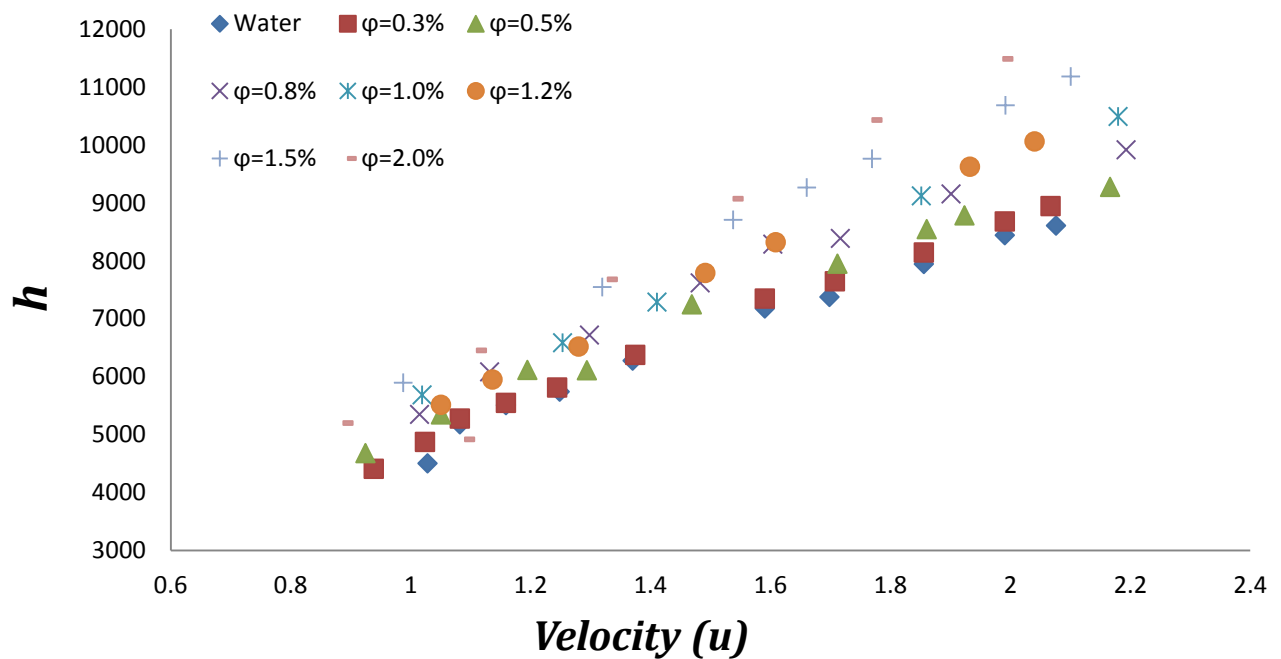


Figure 2-8 : Heat transfer coefficient versus velocity in turbulent flow [26].

As can be seen in Figure 2-8, the convective heat transfer coefficient increases whereas the fluid velocity as well as the nanoparticle concentration increase. All of the nanofluids shown have an increase in the heat transfer coefficient over that of water. Li and Xuan reported that the higher nanoparticle volume fractions, the more sharply viscosity increases, which has adverse effect on heat transfer augmentation in the nanofluid. Hence, it

is important that the proper nanoparticle volume concentration is adopted carefully to achieve heat transfer improvement.

## 2.6 Convective Transport in Nanofluids

Buongiorno [27] introduced seven slip mechanisms that can cause a relative velocity between the nanoparticles and the base fluid: inertia, Brownian diffusion, thermophoresis, diffusiophoresis, Magnus effect, fluid drainage, and gravity. Among these mechanisms, only Brownian diffusion and thermophoresis were found to be important. Buongiorno's analysis consisted of a two-component equilibrium model for mass, momentum, and heat transport in nanofluids. He found that a non-dimensional analysis of the equations implied that energy transfer by nanoparticle dispersion is insignificant, and cannot justify the unusual heat transfer coefficient increases. The boundary layer suggested by Buongiorno has different properties because of the temperature and thermophoresis influences. Consequently the viscosity may decline within boundary layer, in itself, leads to heat transfer augmentation. Taking Brownian motion and thermophoresis into account, Buongiorno developed Eq (2.2) [27] in his paper, for the Nusselt number,

$$Nu_{bf} = \frac{\frac{f}{8} (Re_{bf} - 1000) Pr_{bf}}{1 + \delta_v^+ \sqrt{\frac{f}{8} (Pr_v^{2/3} - 1)}} \leq \quad (2.2)$$

where Nu is the Nusselt number, f is the friction factor, Pr is the Prandtl number, Re is the Reynolds number,  $\delta_v^+$  is the dimensionless thickness of the laminar sublayer, the subscript v represents the laminar sublayer, and the subscript bf represents the base fluid. Buongiorno divides the boundary layer into two layers, the laminar sublayer is closest to the wall, and a

turbulent sublayer is on top of the laminar sublayer. Equation was compared to data from Pak and Cho, and Xuan and Li, works which were previously discussed in this paper. The results are shown in Figure 2-10.

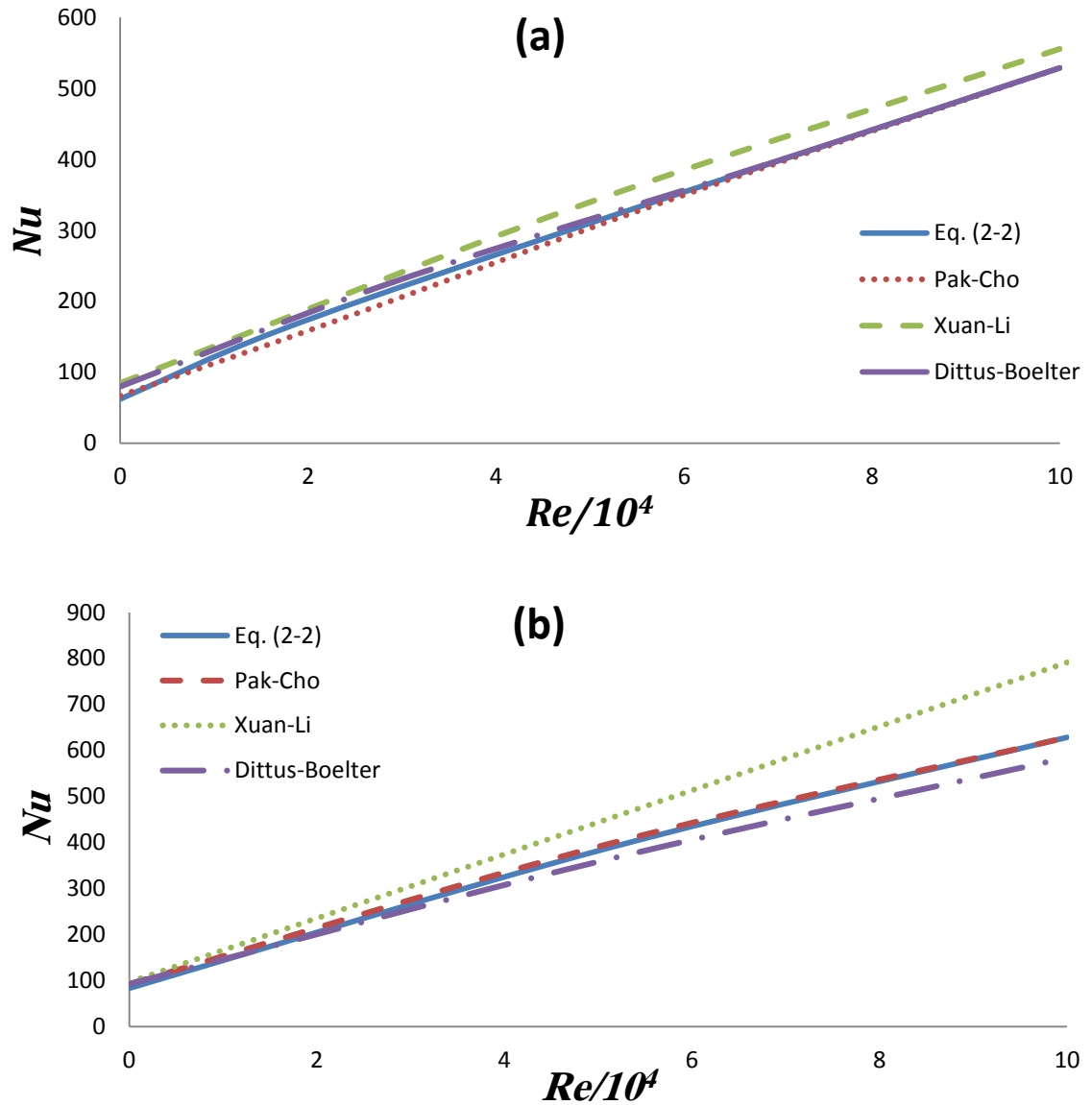


Figure 2-9, Continued

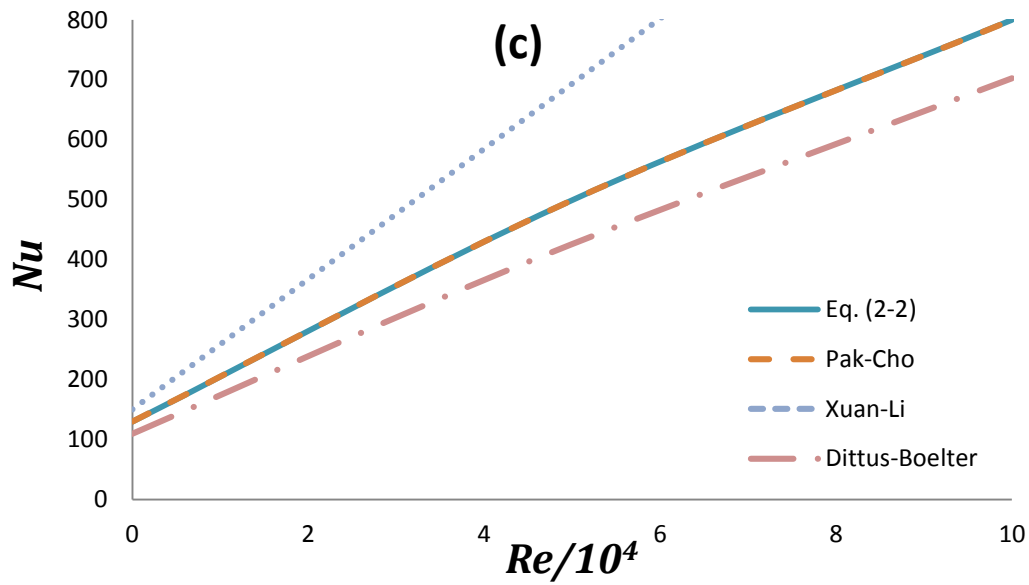


Figure 2-10 : Heat transfer in alumina-water nanofluids: a)  $\phi=0$  b)  $\phi=0.01$  c)  $\phi=0.03$  [27].

Due to the figures, the Nusselt number increases as Reynolds number increases. Equation correlates best with Pak and Cho's experimental data. As the nanoparticle volume fraction is increased, the data from all of the researchers starts to gradually diverge. Correlations for the Nusselt number do not essentially correspond to the correlations for the heat transfer coefficient.

## 2.7 Using water-Nanofluid to improve Heat Transfer for an Electronic Liquid Cooling System

Nguyen et. al. [14] experimentally studied turbulent alumina-water nanofluid as a coolant in microprocessors and other electric systems. They put a liquid cooling block system over a heated block and measured the heat transfer coefficient of the cooling block. Accordingly a noticeable augmentation in the heat transfer coefficient was found by utilizing.

Adding only 6.8% volume concentration of alumina to water leads to the increase of heat transfer coefficient by 40%. They also found that increasing the nanoparticle concentration decreased the heated component temperature. Nguyen, Roy, Gauthier, et. al. employed nanoparticles of 36 nm particle diameter and 47 nm diameter, and concluded that the 36 nm particles produced higher heat transfer coefficients in the water block. Equation (2.3) [14] shows how the heat transfer coefficient of the water block was calculated.

$$q_{\text{electric}} = h_{\text{w-block}} A (T_{\text{m,base}} - T_{\text{m,f}}) \quad (2.3)$$

where  $q_{\text{electric}}$  is the total electric input power,  $h_{\text{w-block}}$  is the heat transfer coefficient of the cooling block,  $A$  is the total increased surface area of the base plate,  $T_{\text{m,base}}$  is the mean temperature of the base plate, and  $T_{\text{m,base}}$  is the average temperature of the fluid going through the block. Figure 2-11 depicts how  $h_{\text{w-block}}$  varies with mass flow rate and nanoparticle volume concentration.

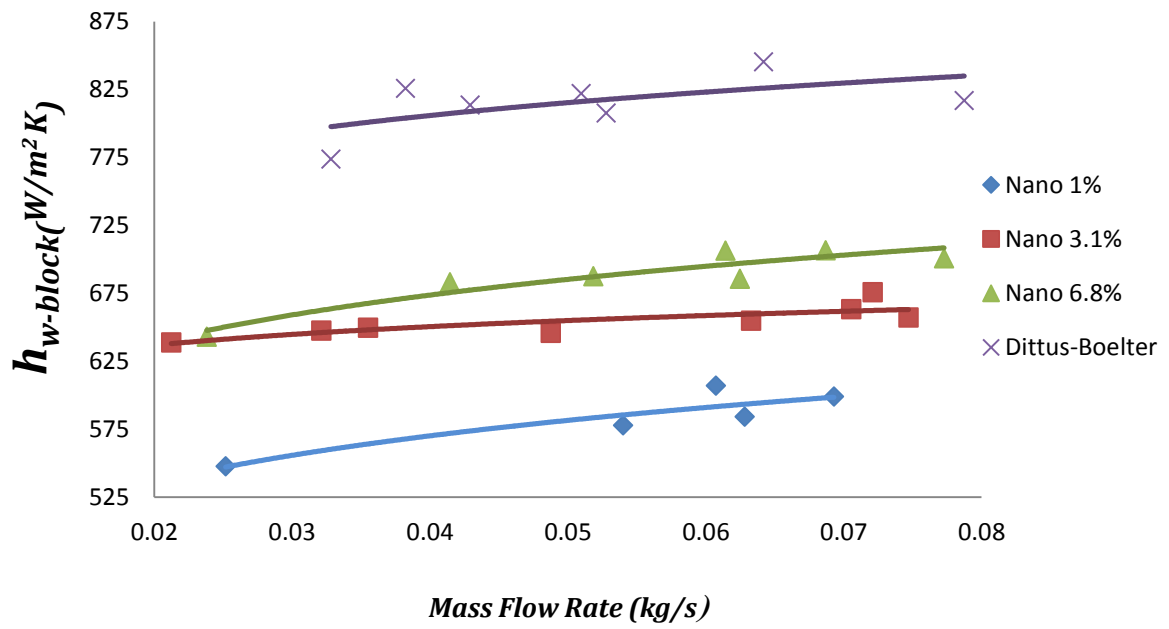


Figure 2-11 : Mass flow rate and particle concentration impacts on the heat transfer coefficient of the water block [14].

As can be seen from Figure 2-11, the addition of nanoparticles has greatly increased the heat transfer coefficient of the water block. At a mass flow rate of 0.07 kg/s, the heat transfer coefficient has been improved by 12%, 18%, and 38% for nanofluids with 1%, 3.1%, and 6.8% nanoparticle concentrations, respectively, compared to the heat transfer coefficient of water. The heat transfer coefficient augmentation is similar for lower mass flow rates as well. As the turbulent flow is strengthened, the heat transfer coefficient increases. Figure 2-12 shows the influence of nanoparticle size on the heat transfer coefficient of the water block.

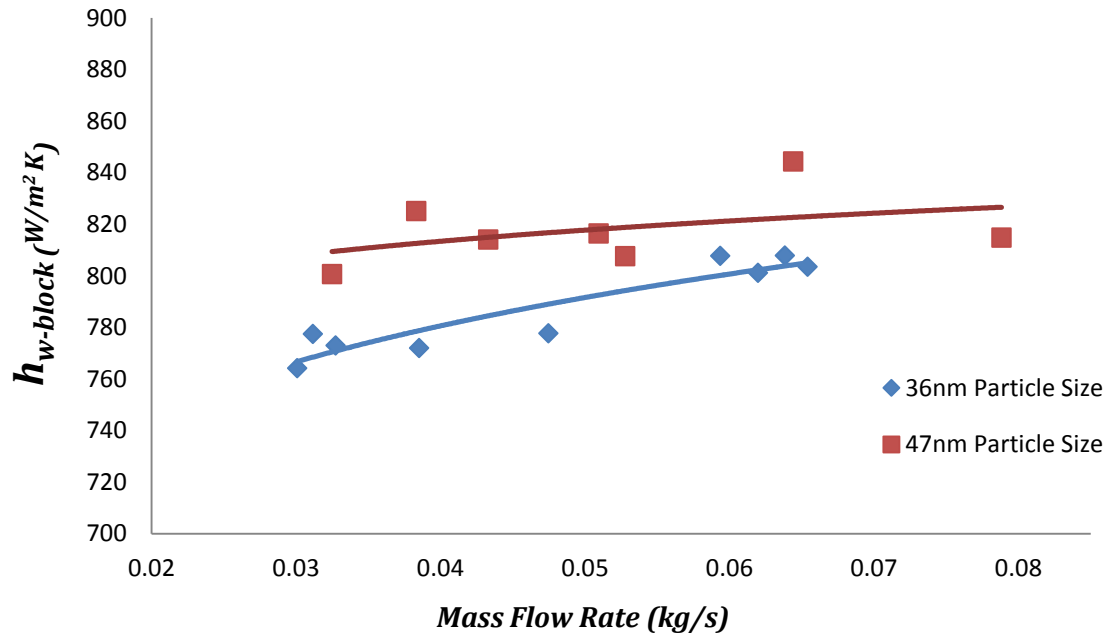


Figure 2-12 : Effect of particle size on  $h_{w-block}$  for 6.8% nanoparticle volume concentration [14].

As one can see from Figure 2-12, the smaller diameter nanoparticles (36 nm) produce a higher water block heat transfer coefficient than the large nanoparticle (47 nm) nanofluid.

## 2.8 Summary of Literature

Most of the research investigated in this chapter was for laminar or turbulent forced convection in a tube. The research summaries presented will not predict the outcomes of this research in terms of numerical results, but they may supply some indication as to what trends to expect.

All of the research studied in this chapter reported increases in heat transfer by using nanoparticles in the base fluid. By what mechanism and to what degree is still arguable.

However, all researchers in general have agreed with the following trends:

- The heat transfer coefficient increases by increasing Reynolds number
- The increment of heat transfer coefficient improve by decreasing size of nanoparticles
- The increment of heat transfer coefficient improve by increasing fluid temperature
- The increment of heat transfer coefficient improve by increasing nanoparticle concentration

# Chapter 3

## 3 METHODOLOGY

The nanofluid consists of CUO and water, and the nanoparticles CUO are assumed to be well dispersed within the base fluid (Water). Furthermore, the nanofluid can be regarded and analyzed as a single-phase fluid because the nanoparticles are ultrafine and they can be fluidized easily. Also, the motions of the nanoparticles can be neglected and the thermal equilibrium state can be assumed to be predominant. Therefore, the following general conservation equations can be used to compute the flow and thermal fields with the effective physical properties of the nanofluid.

### 3.1 Governing Equations of Fluid Dynamics

The fundamental equations of fluid dynamics are based on the following universal laws of conservation:

- Conservation of Mass
- Conservation of Momentum
- Conservation of Energy

The equation that results from applying the conservation of mass law to a fluid flow is called the continuity equation. The conservation of momentum law is nothing more than Newton' Second Law. When this law is applied to a fluid flow, it yields a vector equation

known as the momentum equation. The conservation of Energy law is identical to the first law of Thermodynamics, and the resulting fluid dynamic equation

is named the energy equation [28].

### 3.1.1 Continuity Equation

The conservation of mass law applied to a fluid passing through an infinitesimal fixed control volume  $v$ , (see Figure 3.1) yields the following equation of continuity:

$$\frac{\partial \rho}{\partial t} + \nabla \cdot (\rho \mathbf{V}) = 0 \quad (3.1)$$

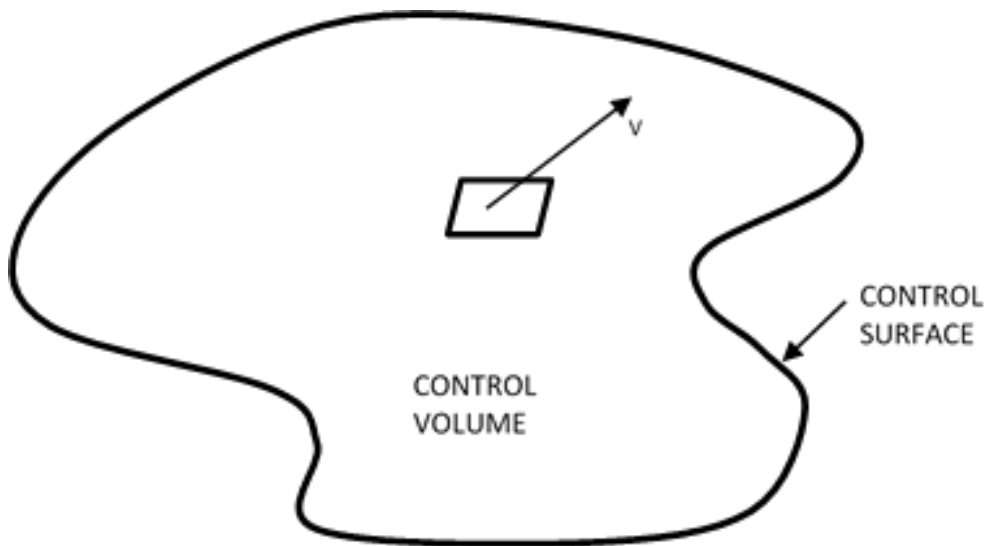


Figure 3-1 Control volume for Eulerian approach [28].

Where  $\rho$  is the fluid density and  $\mathbf{V}$  is the fluid velocity. The first term in this equation represents the rate of increase of the density in the control volume, and the second term represents the rate of mass flux passing out of the control surface (which surrounds the control volume) per unit volume. It is convenient to use the substantial derivative

$$\frac{D(-)}{Dt} \equiv \frac{\partial(-)}{\partial t} + V \cdot \nabla(-) \quad (3.2)$$

to change Equation (3.1) in to the form

$$\frac{D\rho}{Dt} + \rho(\nabla \cdot V) = 0 \quad (3.3)$$

Equation (3.1) was derived using the Eulerian Approach.

For a Cartesian coordinate system, where u, v, w represent the x, y, z components of the velocity vector, Equation (3.1) becomes

$$\frac{\partial \rho}{\partial t} + \frac{\partial}{\partial x}(\rho u) + \frac{\partial}{\partial y}(\rho v) + \frac{\partial}{\partial z}(\rho w) = 0 \quad (3.4)$$

A flow in which the density of each fluid element remains constant is called incompressible.

$$\frac{D\rho}{Dt} = 0 \quad (3.5)$$

which reduces Equation (3.3) to

$$\nabla \cdot V = 0 \quad (3.6)$$

or

$$\frac{\partial u}{\partial x} + \frac{\partial v}{\partial y} + \frac{\partial w}{\partial z} = 0 \quad (3.7)$$

### 3.1.2 Momentum Equation

Newton's second law applied to a fluid passing through an infinitesimal, fixed control volume yields the following momentum equation:

$$\frac{\partial}{\partial t}(\rho V) + \nabla \cdot \rho V V = \rho f + \nabla T \quad (3.8)$$

The first term in this equation represents the rate of increase of momentum per unit volume in the control volume. The second term represents the rate of momentum lost by convection (per unit volume) through the control surface. Note that  $\rho VV$  is a tensor, so that  $\nabla \cdot \rho VV$  is not a simple divergence. This term can be expanded, however, as

$$\nabla \cdot \rho VV = \rho V \cdot \nabla V + V (\nabla \cdot \rho V) \quad (3.9)$$

When this expression for  $\nabla \cdot \rho VV$  is substituted into Equation(3.8), and the resulting equation is simplified using the continuity equation, the momentum equation reduces to

$$\rho \frac{DV}{Dt} = \rho f + \nabla \cdot T_{ij} \quad (3.10)$$

The first term on the right-hand side of Equation (3.10) is the body force per unit volume. In this case, the force per unit mass (f) equals the acceleration of gravity vector g:

$$\rho f = \rho g \quad (3.11)$$

the second term on the right hand side of Equation (3.10) represents the surface forces per unit volume.

the momentum equation given above is quite general and is applicable to both continuum and non-continuum flows.

$$T = -p\delta_{ij} + \mu\left(\frac{\partial u_i}{\partial x_j} + \frac{\partial u_j}{\partial x_i}\right) + \delta_{ij}\mu' \frac{\partial u_k}{\partial x_k}, \quad (i, j, k = 1, 2, 3) \quad (3.12)$$

where  $\delta_{ij}$  is the Kronecker delta function ( $\delta_{ij} = 1$  if  $i=j$  and  $\delta_{ij} = 0$  if  $i \neq j$ );  $u_1, u_2, u_3$  represent the three components of the velocity vector  $\mathbf{V}$ ;  $x_1, x_2$  and  $x_3$  represent the three components of the position vector;  $\mu$  is the coefficient of viscosity (dynamic viscosity), and  $\mu'$  is the second coefficient of viscosity. The two coefficient of viscosity are related to the coefficient of bulk viscosity  $k$  by the expression

$$k = \frac{2}{3}\mu + \mu' \quad (3.13)$$

In general, it is believed that  $k$  is negligible except in the study of the structure of shock wave and in the absorption and attenuation of acoustic waves. For this reason, we will ignore bulk viscosity for the remainder of the text. with  $k=0$ , the second coefficient of viscosity becomes

$$\mu' = -\frac{2}{3}\mu \quad (3.14)$$

and the stress tensor may be written as

$$T = -p\delta_{ij} + \mu\left[\left(\frac{\partial u_i}{\partial x_j} + \frac{\partial u_j}{\partial x_i}\right) - \frac{2}{3}\delta_{ij}\frac{\partial u_k}{\partial x_k}\right] \quad i, j, k = 1, 2, 3 \quad (3.15)$$

the stress tensor is frequently separated in the following manner:

$$T = -p\delta_{ij} + \tau_{ij} \quad (3.16)$$

where  $\tau_{ij}$  represents the viscous stress tensor given by

$$\tau_{ij} = \mu\left[\left(\frac{\partial u_i}{\partial x_j} + \frac{\partial u_j}{\partial x_i}\right) - \frac{2}{3}\delta_{ij}\frac{\partial u_k}{\partial x_k}\right] \quad i, j, k = 1, 2, 3 \quad (3.17)$$

upon substituting Equation (3.15) into (3.10), the famous Navier-stokes equation is obtained:

$$\rho \frac{DV}{Dt} = \rho f - \nabla p + \frac{\partial}{\partial x_j} \left[ \mu \left( \frac{\partial u_i}{\partial x_j} + \frac{\partial u_j}{\partial x_i} \right) - \frac{2}{3} \delta_{ij} \mu \frac{\partial u_k}{\partial x_k} \right] \quad (3.18)$$

For a Cartesian coordinate system, Equation (3.18) can be separated into the following three scalar Navier-Stokes equations:

$$\rho \frac{Du}{Dt} = \rho f_x - \frac{\partial p}{\partial x} + \frac{\partial}{\partial x} \left[ \frac{2}{3} \mu \left( 2 \frac{\partial u}{\partial x} - \frac{\partial v}{\partial y} - \frac{\partial w}{\partial z} \right) \right] + \frac{\partial}{\partial y} \left[ \mu \left( \frac{\partial u}{\partial y} + \frac{\partial v}{\partial x} \right) \right] + \frac{\partial}{\partial z} \left[ \mu \left( \frac{\partial w}{\partial x} + \frac{\partial u}{\partial z} \right) \right] \quad (3.19)$$

$$\rho \frac{Dv}{Dt} = \rho f_y - \frac{\partial p}{\partial y} + \frac{\partial}{\partial x} \left[ \mu \left( \frac{\partial v}{\partial x} + \frac{\partial u}{\partial y} \right) \right] + \frac{\partial}{\partial y} \left[ \frac{2}{3} \mu \left( 2 \frac{\partial v}{\partial y} - \frac{\partial u}{\partial x} - \frac{\partial w}{\partial z} \right) \right] + \frac{\partial}{\partial z} \left[ \mu \left( \frac{\partial v}{\partial z} + \frac{\partial w}{\partial y} \right) \right] \quad (3.20)$$

$$\rho \frac{Dw}{Dt} = \rho f_z - \frac{\partial p}{\partial z} + \frac{\partial}{\partial x} \left[ \mu \left( \frac{\partial w}{\partial x} + \frac{\partial u}{\partial z} \right) \right] + \frac{\partial}{\partial y} \left[ \mu \left( \frac{\partial v}{\partial z} + \frac{\partial w}{\partial y} \right) \right] + \frac{\partial}{\partial z} \left[ \frac{2}{3} \mu \left( 2 \frac{\partial w}{\partial z} - \frac{\partial u}{\partial x} - \frac{\partial v}{\partial y} \right) \right] \quad (3.21)$$

If the flow is incompressible and the coefficient of viscosity  $\mu$  is assumed constant, Eq. (3.18) will reduce to much simpler form

$$\rho \frac{DV}{Dt} = \rho f - \nabla p + \mu \nabla^2 V \quad (3.22)$$

### 3.1.3 Equation of Energy

The first law of thermodynamic applied to a fluid passing through an infinitesimal; fixed control volume yields the follow energy equation[28]:

$$\frac{\partial E_t}{\partial t} + \nabla \cdot EV = \frac{\partial Q}{\partial t} - \nabla \cdot q + \rho f \cdot v + \nabla \cdot (T_{ij} \cdot V) \quad (3.23)$$

Where  $E_t$  is the total energy per unit volume given by

$$E_t = \rho \left( e + \frac{V^2}{2} \text{potential energy} + \dots \right) \quad (3.24)$$

and  $e$  is the internal energy per unit mass. The first term on the left-hand side of Equation (3.23) represents the rate of increase of  $E_t$  in the control volume, while the second term represents the rate of total energy lost by convection (per unit volume) through the control surface. The first term on the right hand side of Equation (3.23) is the rate of heat produced per unit volume by external agencies, while the second term  $(\nabla \cdot q)$  is the rate of heat lost by conduction (per unit volume) through the control surface. Fourier's law for heat transfer by conduction will be assumed, so that the heat transfer  $q$  can be expressed as

$$Q = -k \nabla T \quad (3.25)$$

where  $k$  is the coefficient of thermal conductivity and  $T$  is the temperature. The third term on the right hand side of Equation (3.23) represents the work done on the control volume (per unit volume) by the body forces, while the fourth term represents the work done on the control volume (per unit volume) by the surface forces. It should be obvious that Equation (3.23) is simply the first law of thermodynamics applied to the control volume. That is, the increase of energy in the system is equal to heat added to the system plus the work done on the system.

For Cartesian coordinate system, Equation (3.23) becomes

$$\begin{aligned} \frac{\partial E_t}{\partial t} - \frac{\partial Q}{\partial t} - \rho (f_x u + f_y v + f_z w) + \frac{\partial}{\partial x} (E_t u + p u - u \tau_{xx} - v \tau_{xy} - w \tau_{xz} + q_x) \\ + \frac{\partial}{\partial y} (E_t v + p v - u \tau_{xy} - v \tau_{yy} - w \tau_{yz} + q_y) \\ + \frac{\partial}{\partial z} (E_t w + p w - u \tau_{xz} - v \tau_{yz} - w \tau_{zz} + q_z) = 0 \end{aligned} \quad (3.26)$$

which is in conservation law form. Using the continuity equation, the left hand side of Equation (3.23) can be replaced by the follow expression:

$$\rho \frac{D(E_t / \rho)}{Dt} = \frac{\partial E_t}{\partial t} + \nabla \cdot E_t V \quad (3.27)$$

which is equivalent to

$$\rho \frac{D(E_t / \rho)}{Dt} = \rho \frac{De}{Dt} + \rho \frac{D(V^2 / 2)}{Dt} \quad (3.28)$$

if only internal energy and kinetic energy are considered significant in Eq. (3.24). Forming the scalar dot product of Eq. (3.10) with the velocity vector  $V$  allows one to obtain

$$\rho \frac{DV}{Dt} \cdot V = \rho f \cdot V - \nabla p \cdot V + (\nabla \cdot \tau_{ij}) \cdot V \quad (3.29)$$

Now if Eq. (3.27), (3.28) and (3.29) are combined and substituted into Eq. (3.23), a useful variation of the original energy equation is obtained:

$$\rho \frac{De}{Dt} + p(\nabla \cdot V) = \frac{\partial Q}{\partial t} - \nabla \cdot q + \nabla \cdot (\tau_{ij} \cdot V) - (\nabla \cdot \tau_{ij}) \cdot V \quad (3.30)$$

the last two terms in this equation can be combined into a single term, since

$$\tau_{ij} \frac{\partial u_i}{\partial x_j} = \nabla \cdot (\tau_{ij} \cdot V) - (\nabla \cdot \tau_{ij}) \cdot V \quad (3.31)$$

and it becomes

$$\rho \frac{De}{Dt} + p(\nabla \cdot V) = \frac{\partial Q}{\partial t} - \nabla \cdot q \quad (3.32)$$

if the flow is incompressible, and if the coefficient of thermal conductivity assumed constant,

Eq. (3.32) reduces to

$$\rho \frac{De}{Dt} = \frac{\partial Q}{\partial t} + k \nabla^2 T \quad (3.33)$$

### **3.2 Finite Volume Method (FVM)**

The FVM to solve the governing equations can be classified into the mixed interpolation methods, the penalty methods, and the segregated velocity pressure solution methods. The segregated scheme adopted in the present study requires much less execution time and storage than the other two methods, particularly for the three-dimensional configurations. Also, the pressure is computed only once in the stage of the pressure correction without iterative calculations [29].

The numerical algorithm by FVM is shown in Figure 3-2. The velocity and the pressure are obtained from the continuity and momentum equations through the four stages of the solution procedures. The segregated approaches consist of convective approximation, viscous prediction, pressure correction, and velocity correction. The temperature is acquired from the energy equation through the two stages: the convective approximation and the diffusive prediction. When the temperature is calculated, the velocity is also required in the energy equation [30-32].

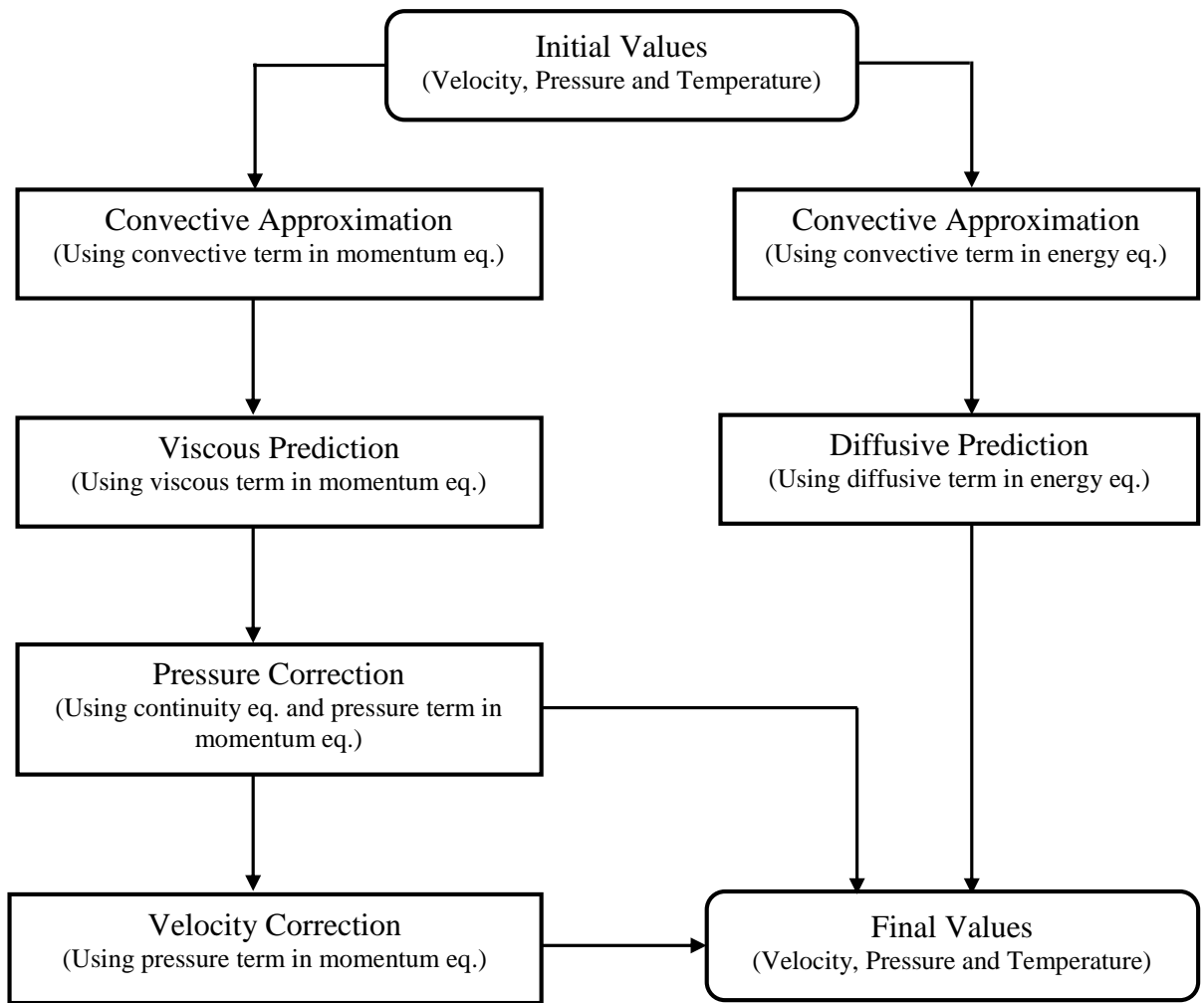


Figure 3-2 : The numerical algorithm by FVM is shown [33]

### 3.3 Geometric shape and Boundary conditions

The geometrical configuration of the pipes with the return bend is shown in Figure 3-3. The diameter ( $d$ ) of the pipe is given 10 (mm) and the lengths ( $l$ ) of inlet and outlet pipes are set up to 10 times the length of the diameter. Also, the curvature radius ( $R$ ) of the return bend is 1.5 times of the diameter.

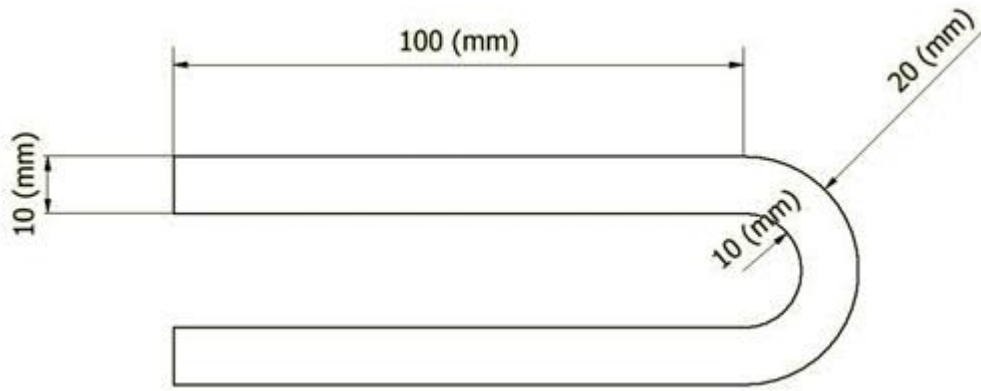


Figure 3-3 : Schematic representation for cross section of pipes with return bend.

The inlet boundary conditions are the velocities in the axial direction for different Reynolds Numbers and the temperature,  $T=300^{\circ}\text{K}$ , as illustrated in Figure 3-5.

Meanwhile, the geometric coordinate values of the pipes with the return bend are obtained from a straight pipe by using coordinate transformations. The numerical solutions are calculated until the iteration is conducted up to 500 times, which is the calculation condition that reaches to the steady state.

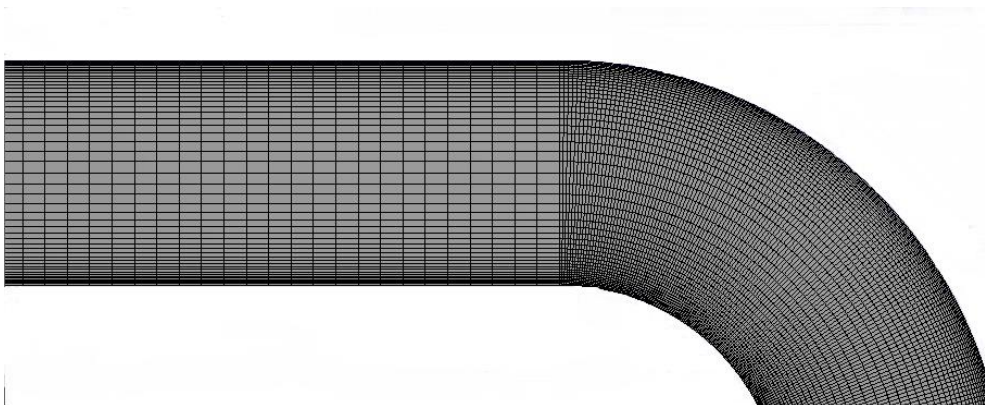


Figure 3-4 : Grid sample used in this study

The relatively fine grids are used in the regions of the inlet and the return bend. The grid points of 25551 and the elements of 25000 are used in the pipes.

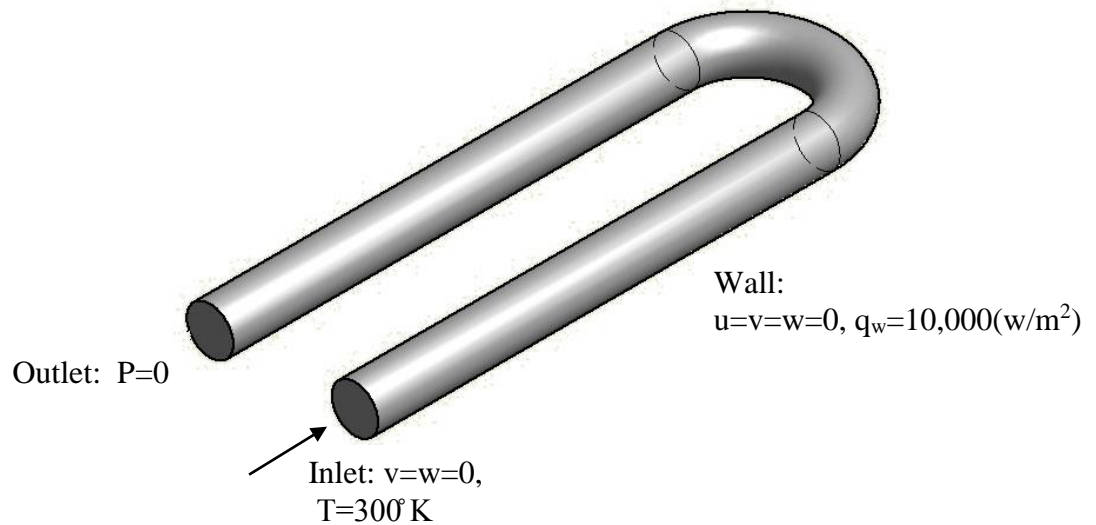


Figure 3-5 : Boundary conditions for pipes with return bend.

The physical properties of water and CUO are shown in Table 3-1, and the effective physical properties of the nanofluids are obtained from the physical properties of the base fluid (water) and the nanoparticles (CUO), respectively. The CUO-water nanofluid is expected to have the enhanced heat transfer characteristics since the thermal conductivity of CUO is much higher than that of water.

Table 3-1 : Physical properties of water and CUO.

	Density ( $\text{Kg/m}^3$ )	Viscosity ( $\text{Ns/m}^2$ )	Specific heat ( $\text{J/Kg K}$ )	Conductivity ( $\text{W/m K}$ )	Shape factor ( $n$ )
<b>Water</b>	998.0	$1.002 \times 10^{-3}$	4182.0	0.5984	-
<b>CUO</b>	6500	-	535.6	20	3

The effective physical properties of the nanofluid are obtained as functions of nanoparticle volume concentration ( $\phi$ ) [34]:

$$\rho_{eff} = (1-\phi)\rho_f + \phi\rho_s \quad (3.34)$$

$$\mu_{eff} = (123\phi^2 + 7.3\phi + 1)\mu_f \quad (3.35)$$

$$(C_p)_{eff} = \left[ \frac{(1-\phi)(\rho C_p)_f + \phi(\rho C_p)_s}{(1-\phi)\rho_f + \phi\rho_s} \right] \quad (3.36)$$

$$k_{eff} = \left( \frac{k_s + (n-1)k_f - (n-1)\phi(k_f - k_s)}{k_s + (n-1)k_f - \phi(k_f - k_s)} \right) k_f \quad (3.37)$$

The Equation (3.35) of the effective viscosity was obtained by performing a least-square curve fitting of experimental data available for the mixtures [35]. Also, the Equation (3.37) of the effective thermal conductivity was introduced by Hamilton and Crosser [36, 37]. Here, the concentration of 0% means the pure water in which the nanoparticles are not included within. The values of effective properties used in this work are tabulated in Table 3-2 [37].

Table 3-2 : Variations of effective physical properties with concentration.

Concentration	Density (kg/m <sup>3</sup> )	Viscosity (Ns/m <sup>2</sup> )	Specific heat (J/kgK)	Conductivity (W/mK)
0%	998	0.001002000	4182	0.5984
2%	1108.236	0.001237756	3754.264391	0.681617479
4%	1218.272	0.001637003	3403.796118	0.719140264
6%	1328.308	0.002434775	3111.392882	0.757301975
8%	1438.344	0.004795963	2863.728432	0.796600211

### 3.4 Validation results

The straight pipe with the diameter of 10 millimetres and the length of 2000 millimetres are used for the numerical analysis. The meshing of the straight pipe consists of the nodal points of 62031 and the number of elements is 60000 for the Fluent.

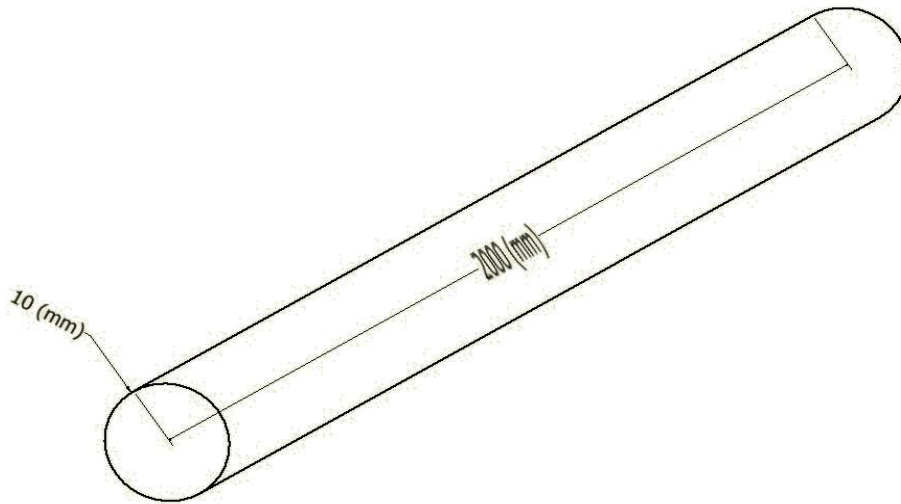


Figure 3-6 : Use straight pipe and water to comparison numerical with analytic results.

Table 3-3 : Boundary conditions in straight pipe.

<b>Boundary conditions</b>	
<b>Inlet</b>	$V=W=0$ , $T=300$ k
<b>Outlet</b>	$P=0$
<b>Wall</b>	$u = v = w = 0$ , $q_w = -k(\partial T^* / \partial r) = 0.5(W/m^2)$

For the straight pipe, the boundary conditions are shown in Table 3-3. At The inlet the, temperature is set up to 300° K and at the wall boundary the velocities  $u$ ,  $v$  and  $w$  are 0 and the uniform heat flux ( $q_w$ ) is 0.5 (W/m<sup>2</sup>). The numerical analysis is performed at the various Reynolds numbers. The calculation is conducted until the iteration is performed up to 1000, which is the calculation condition that reaches to the steady state.

The temperature profiles calculated by the Ansys fluent and the analytic equation are shown in Figure 3-7. The temperature is calculated by the formula almost coincide with the results from the Fluent with time. The analytic solution for the straight pipe is gained by

$$T_m(x) = T_{m_i} + \left( \frac{q \times p}{\dot{m} \times C_p} \right) x \quad (3.38)$$

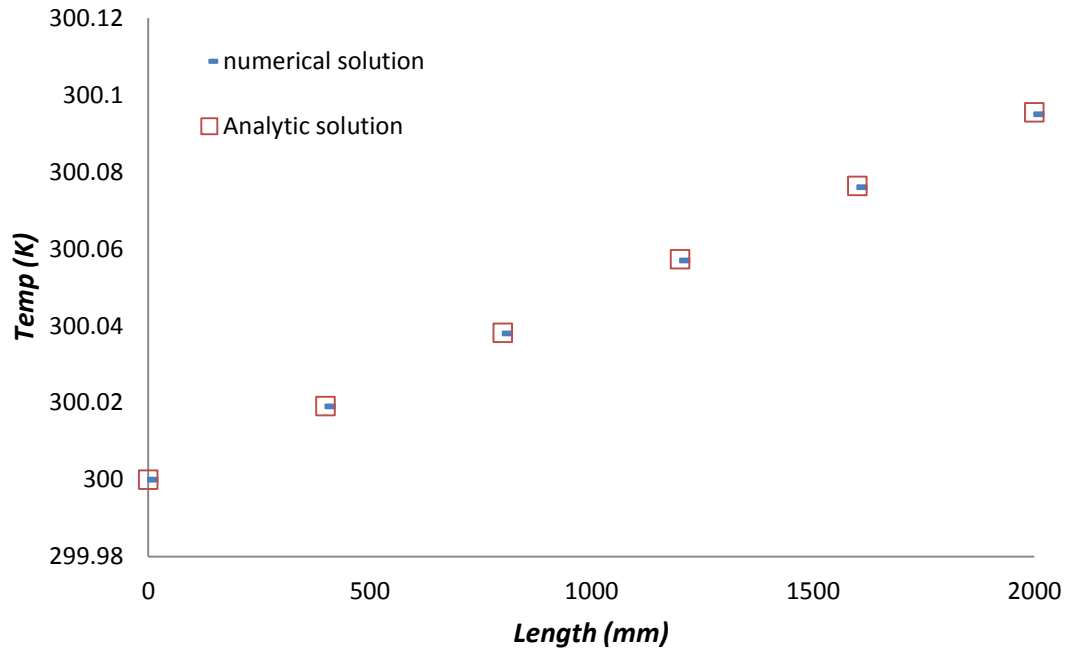


Figure 3-7 : Temperature profiles through straight pipe.

The Nusselt numbers calculated by the Fluent and by the analytic solutions are presented in Figure 3-8 and Table 3-4. The Nusselt numbers in the region of the fully developed flow is 4.38 and 4.36 are gained by the Fluent and the analytic solutions, respectively. There is an error of 0.45% in the numerical solution and this difference is believed to be the mesh size effect. As a result, the numerical solutions by the ANSYS Fluent are acceptable and can be used in the numerical analysis for the nanofluid flow through the 180° curve.

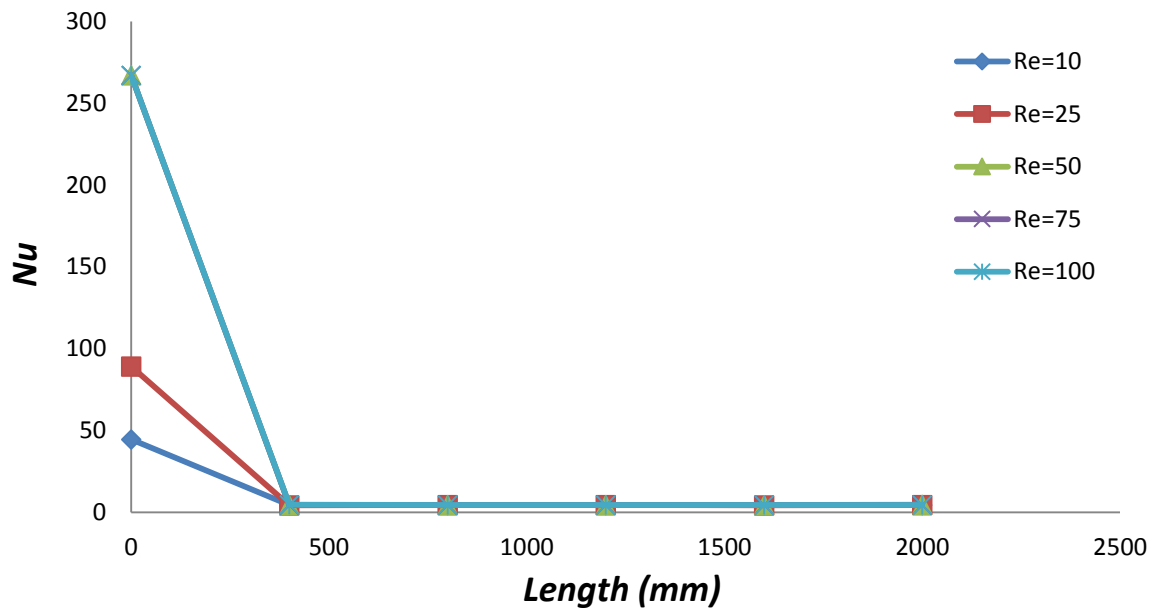


Figure 3-8 : Nusselt profiles for various Reynolds numbers through pipe.

Table 3-4 : Nusselt numbers for various Reynolds numbers through pipe.

<b>X (mm)</b>	<b>Re=10</b>	<b>Re=25</b>	<b>Re=50</b>	<b>Re=75</b>	<b>Re=100</b>	<b>Analytical Nu</b>
<b>0</b>	44.5459	89.0919	267.276	267.276	267.276	4.36
<b>400</b>	4.4546	4.3109	4.38157	4.4546	4.5301	4.36
<b>800</b>	4.38157	4.4546	4.4546	4.4546	4.4546	4.36
<b>1200</b>	4.38157	4.38157	4.4546	4.4546	4.4546	4.36
<b>1600</b>	4.38157	4.3109	4.38157	4.4546	4.4546	4.36
<b>2000</b>	4.3821	4.38157	4.55238	4.4765	4.4765	4.36

# Chapter 4

## 4 RESULTS AND ANALYSIS

The numerical analysis for the hydrodynamic and thermal flows of nanofluid in the pipes with the return bend has been performed with different concentrations and Reynolds numbers. In total, the 25 cases have been simulated in the conditions of the concentrations of 0%, 2%, 4%, 6%, and 8% and the Reynolds numbers of 100, 250, 500, 750, and 1000, respectively. For better understanding the thermal and fluid flows in the return bend, the dimensionless velocity and temperature distributions at the concentration of 0% are shown in Figure 4-1 and Figure 4-2 when the Reynolds numbers are 10 and 1000, respectively.

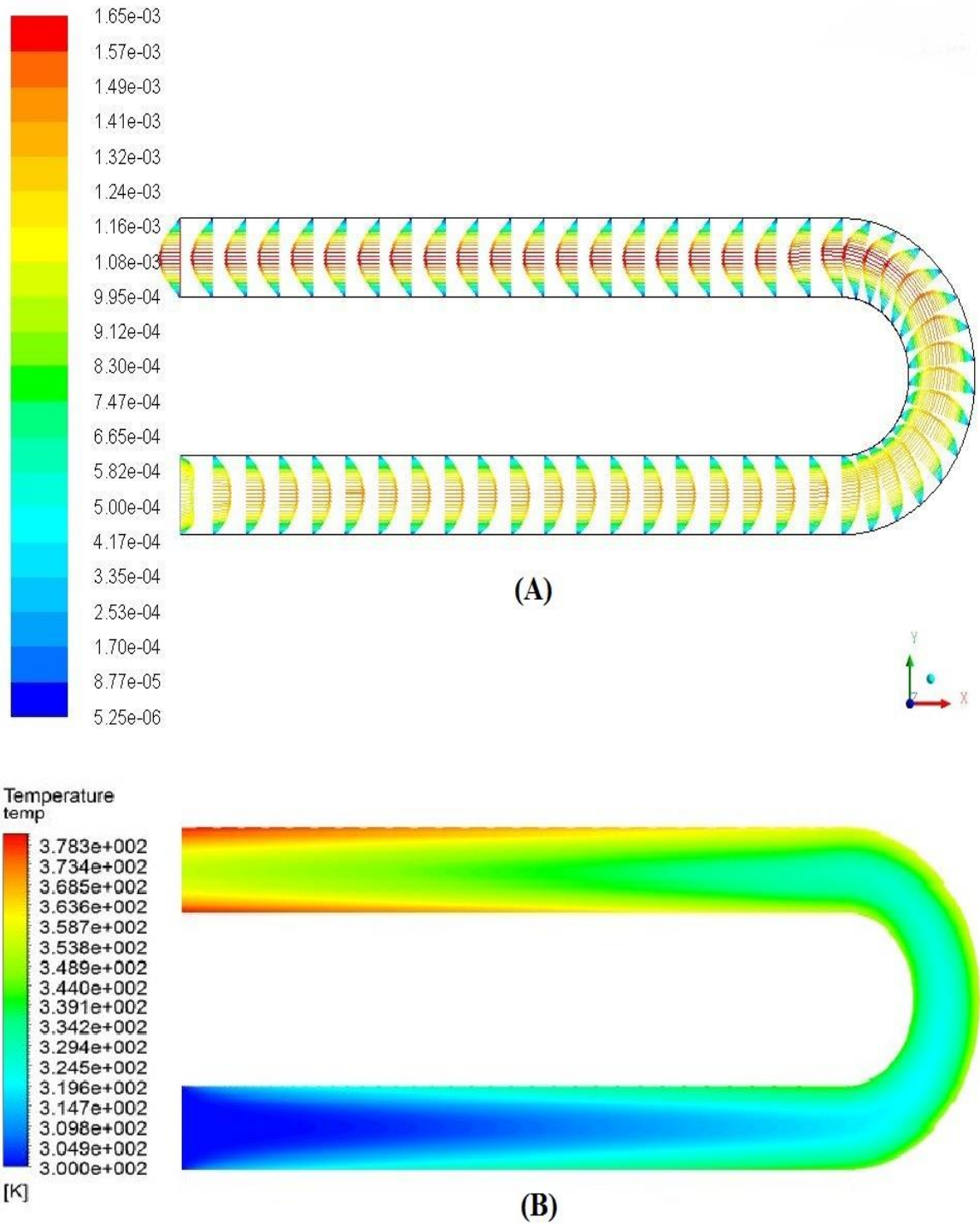


Figure 4-1 : Distributions of velocity (A) and temperature (B) of water at  $Re=10$ .

The velocity profiles at the Reynolds number of 10 keep nearly parabolic shapes in the entire pipes.

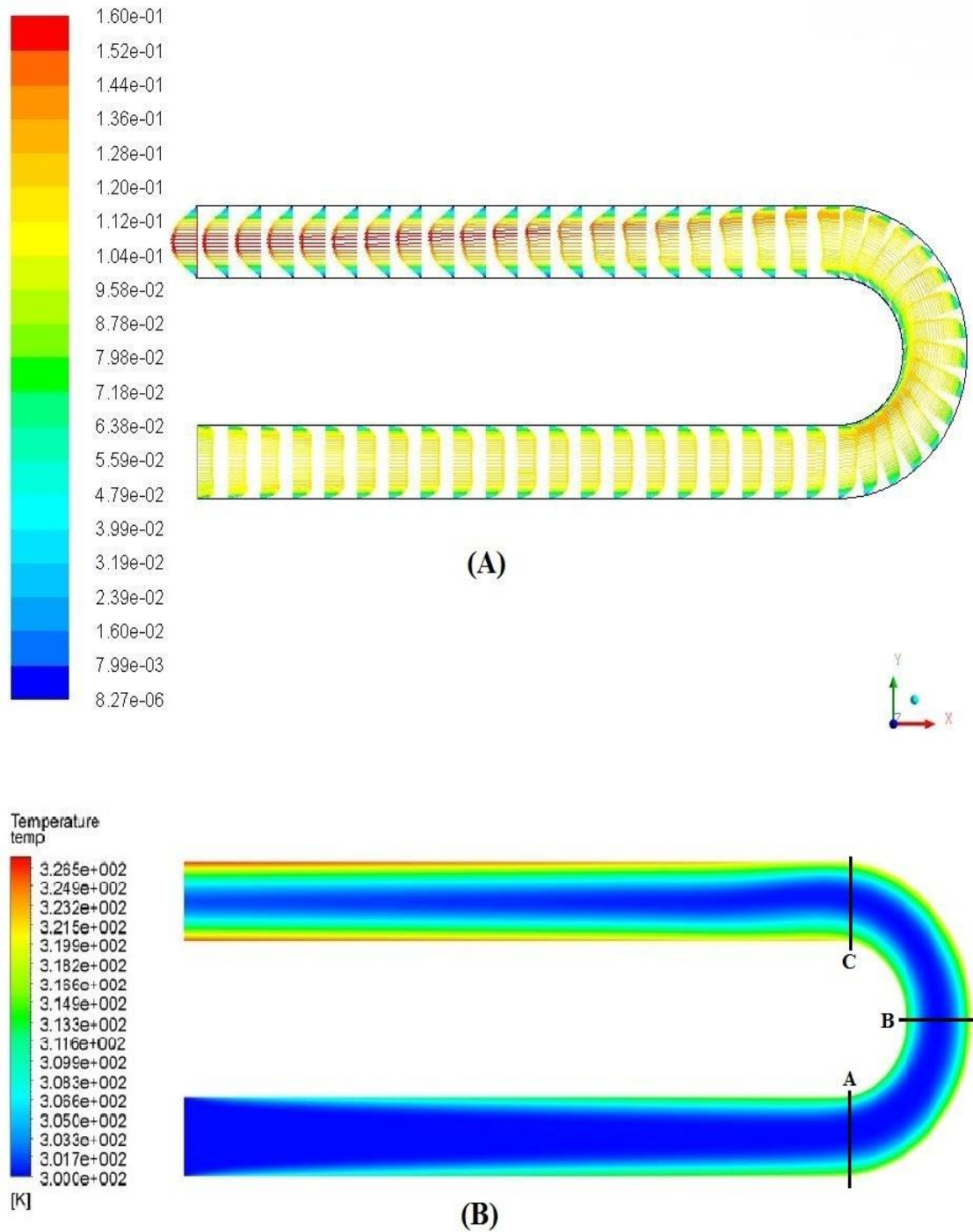


Figure 4-2 : Distributions of velocity (A) and temperature (B) of water at  $Re=1000$ .

However, at the Reynolds number of 1000, at first the velocity in the inner region of the return bend appears higher than that in the outer region and then flow is changed. Figure 4-3 shows the path of maximum velocity before  $90^\circ$  is at the near the inner region and after about  $90^\circ$  maximum velocity is near outer region. This flow can affect the heat transfer characteristics in the return bend and in the outlet pipe. Also, the heat transfer is expected to be improved between the inside and the outside of the pipe because the cold flow in the core of the inlet pipe shifts to the outer region of the return bend as shown in Figure 4-2 and Figure 4-3.

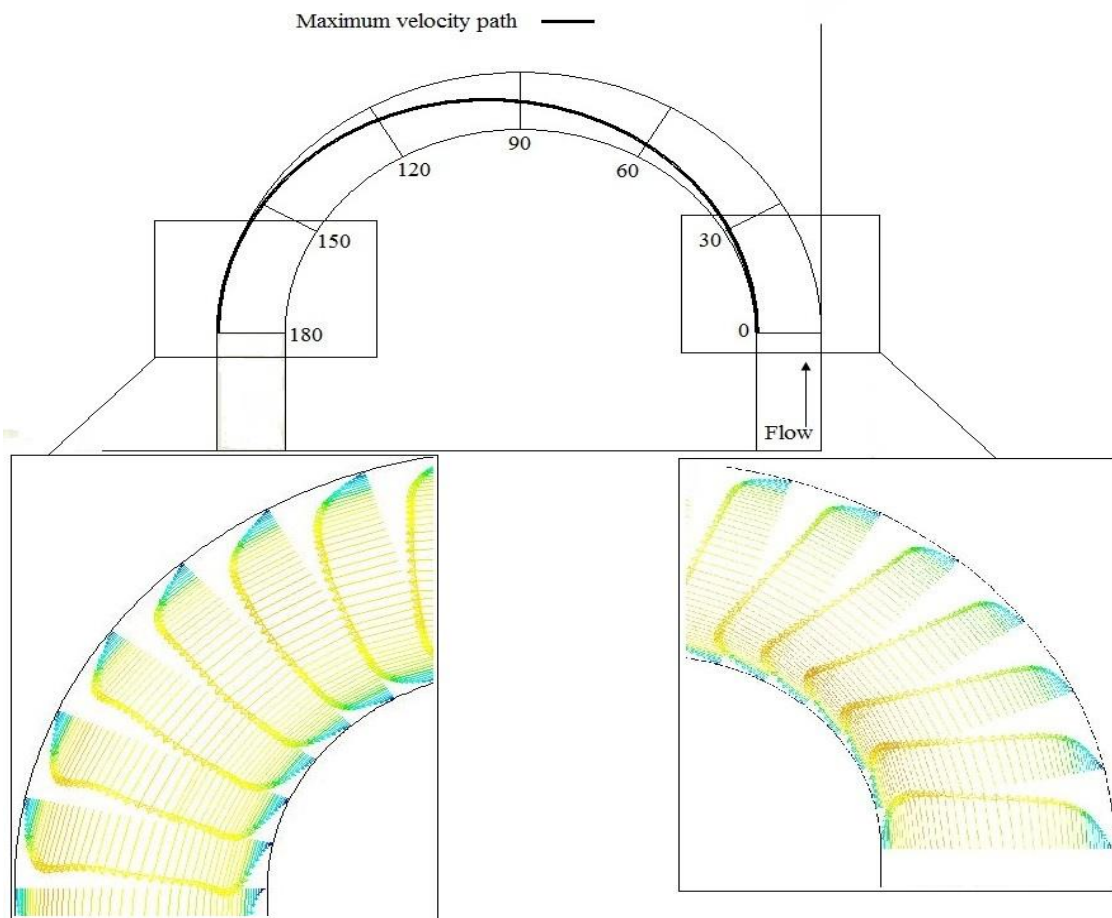


Figure 4-3 : shows the path of maximum velocity through the curve.

The velocity and temperature profiles for at the cross sections A, B and C are represented in Figure 4-4, Figure 4-5 and Figure 4-6.

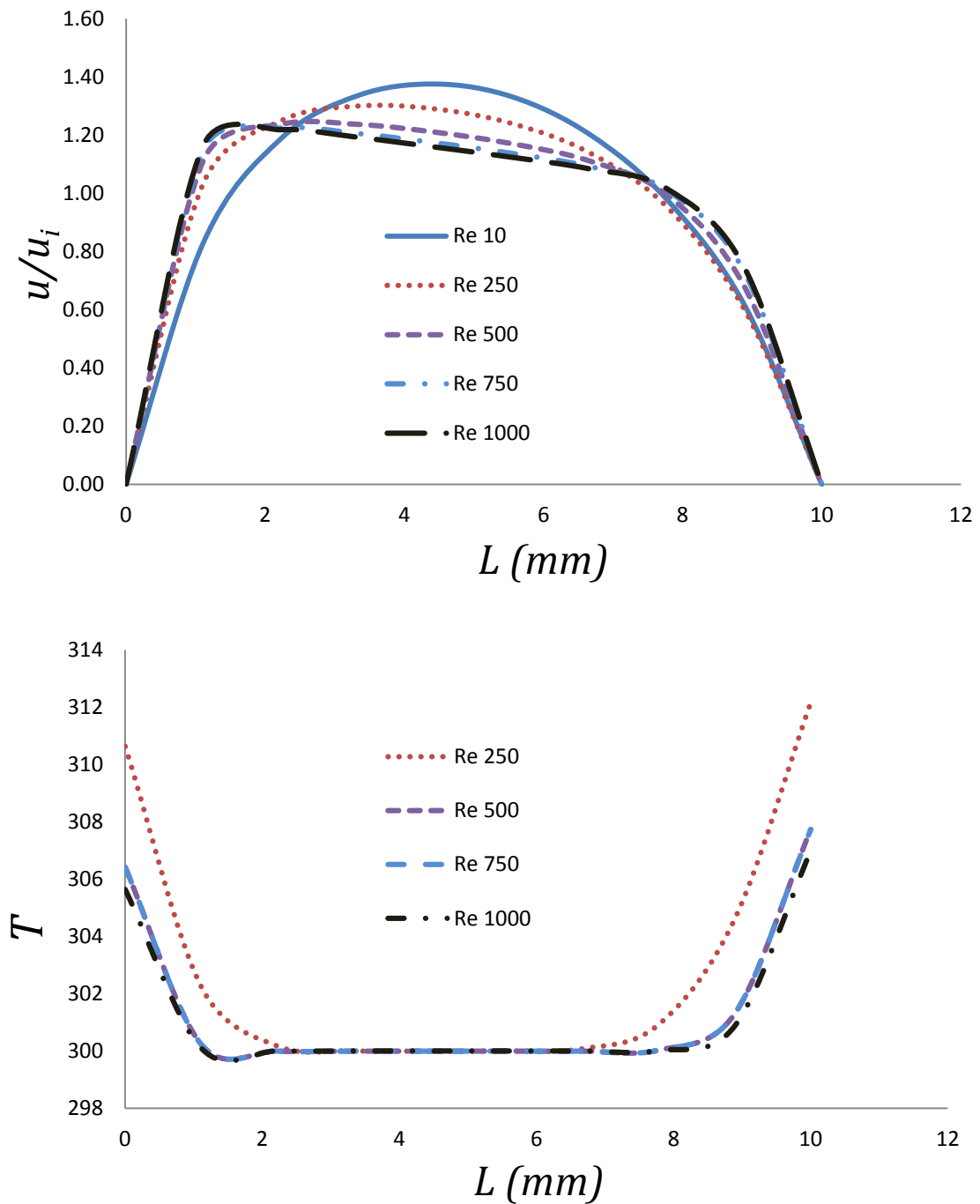


Figure 4-4 : Dimensionless velocity and Temperature profiles at various Reynolds numbers at section (A).

The position of the maximum velocity is moved towards the outer region of the return bend as the Reynolds number increases. The temperature at the wall of the return bend is higher than that at the centre as shown in Figure 4-5(B) and Figure 4-6(B) because the heat flux is uniformly supplied at the wall boundary. However, as the Reynolds number increases, the temperature declines gradually in the outer region of the return bend due to the cold flow from the inlet pipe.

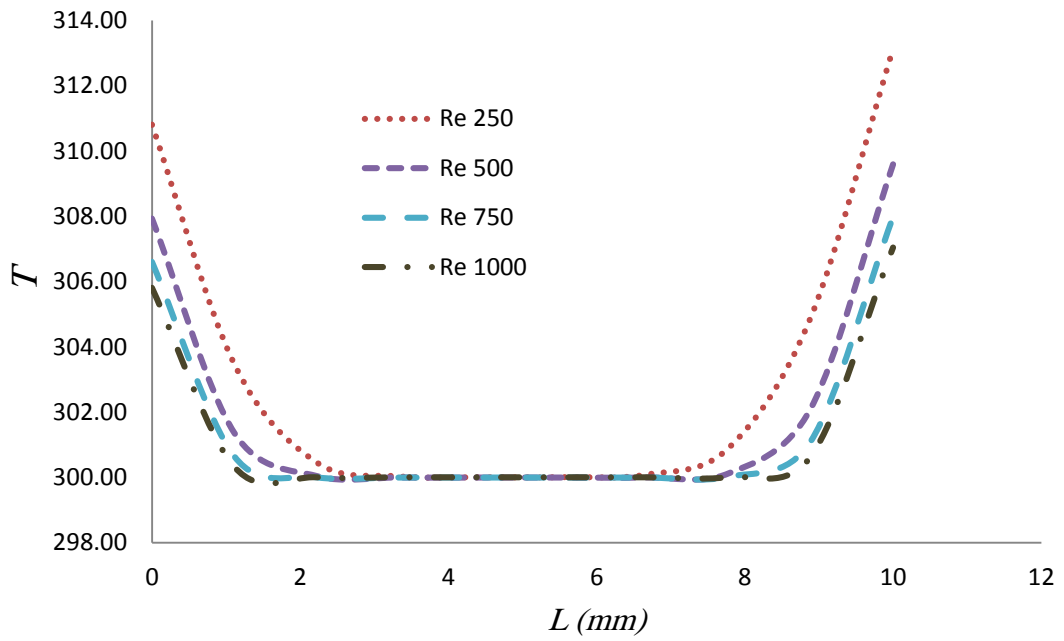
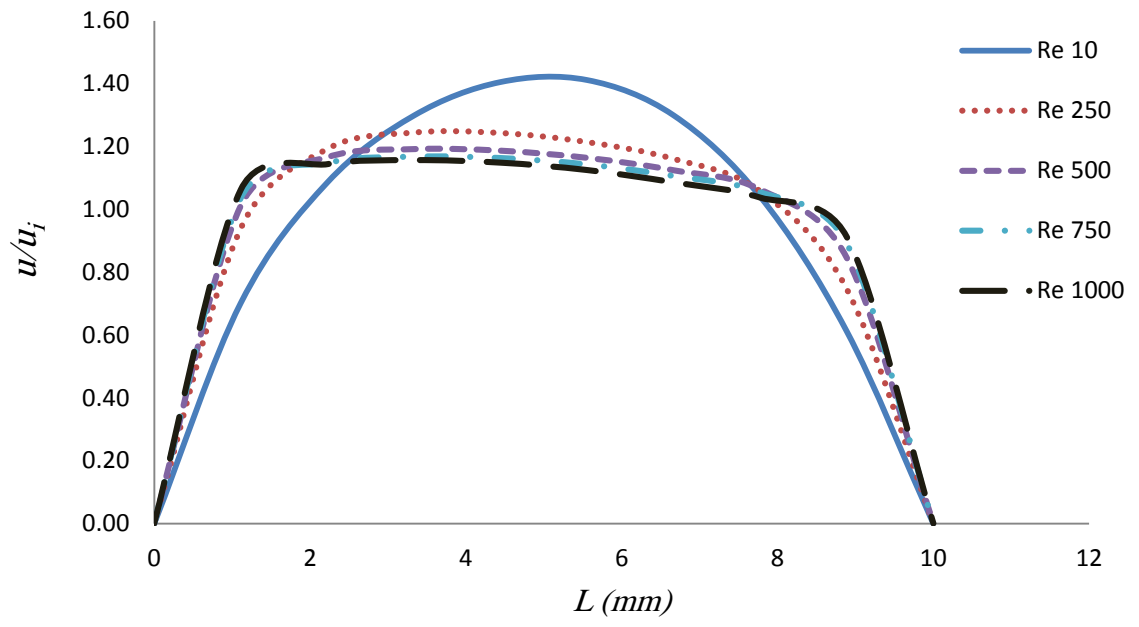


Figure 4-5. Temperature and Dimensionless velocity profiles at various Reynolds numbers at section (B).

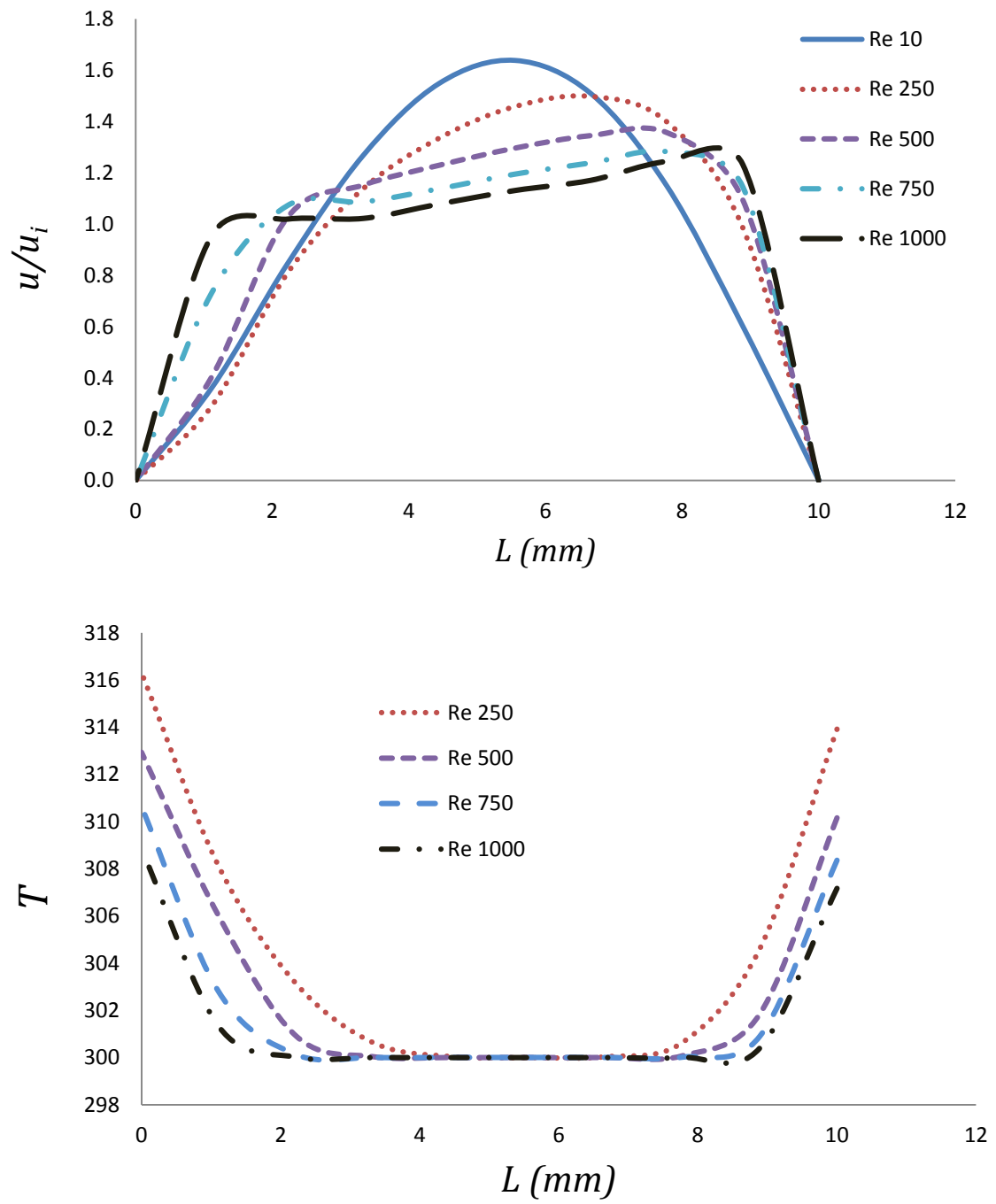


Figure 4-6 : Temperature and Dimensionless velocity profiles at various Reynolds numbers at section (C).

The centrifugal force causes the secondary flow occurs through the curve. In other words, because of the changed centrifugal forces between in the inner and outer regions, there are two rotating flows at the top and bottom of the curve [2].

In detail, it can be seen by increase of the Reynolds number the cold flow moves to the outer region. The temperature distribution at the top of curve is lower than that at the bottom because the amount of the secondary flow increased slowly.

To look into the role of 180 degree curve, the whole pipes are divided into three parts: the inlet pipe, outlet pipe and the return bend. The average Nusselt numbers at the concentration of 0% are obtained with the Reynolds number increasing as revealed in Figure 4-7. Although the slopes appear different, the average Nusselt numbers rise in all parts because the inlet velocity increases with increasing Reynolds number. At the Reynolds numbers of 100, 250, 500, 750, and 1000, the average Nusselt numbers of the return bend are larger than those of the inlet and outlet pipes because the cold flow in the inlet pipe moves to the outer region of the return bend as shown in Figure 4-1 Figure 4-2. In other words, the heat transfer in the return bend improves with the increase of the Reynolds number due to the secondary flow.

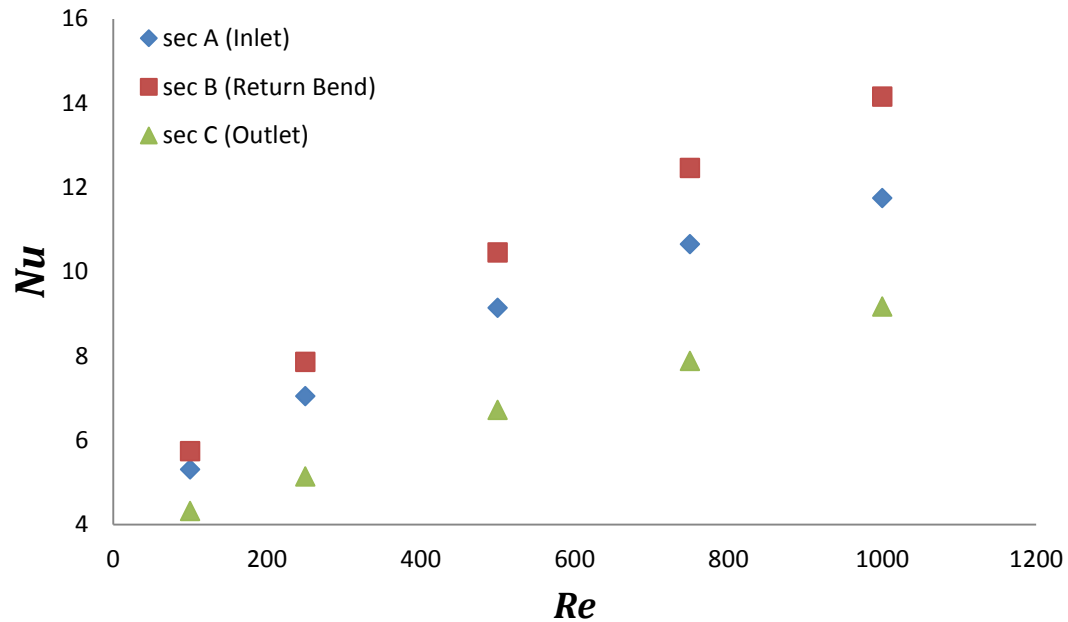


Figure 4-7 : Comparisons of average Nusselt numbers in various parts.

Figure 4-8 shows the average Nusselt numbers at different Reynolds numbers of 100, 250, 500, 750, and 1000 and concentrations of 0%, 2%, 4%, 6%, and 8%, respectively. The average Nusselt numbers increase with the rise of the Reynolds number and the concentration. In general, the heat transfer of the nanofluid is improved with the augmentation of the concentration because the thermal conductivity of the nanofluid grows with the concentration as shown in Table 3-2. In addition, the increment of the concentration is accompanied by the rise of the inlet velocity at the same Reynolds number as expressed in Table 4-1. Therefore, these conditions cause the increase of the average Nusselt number. It is noted that the results at the concentration of 8% might not be correct in reality because the stable nanofluid could not be found for such high volume concentrations.

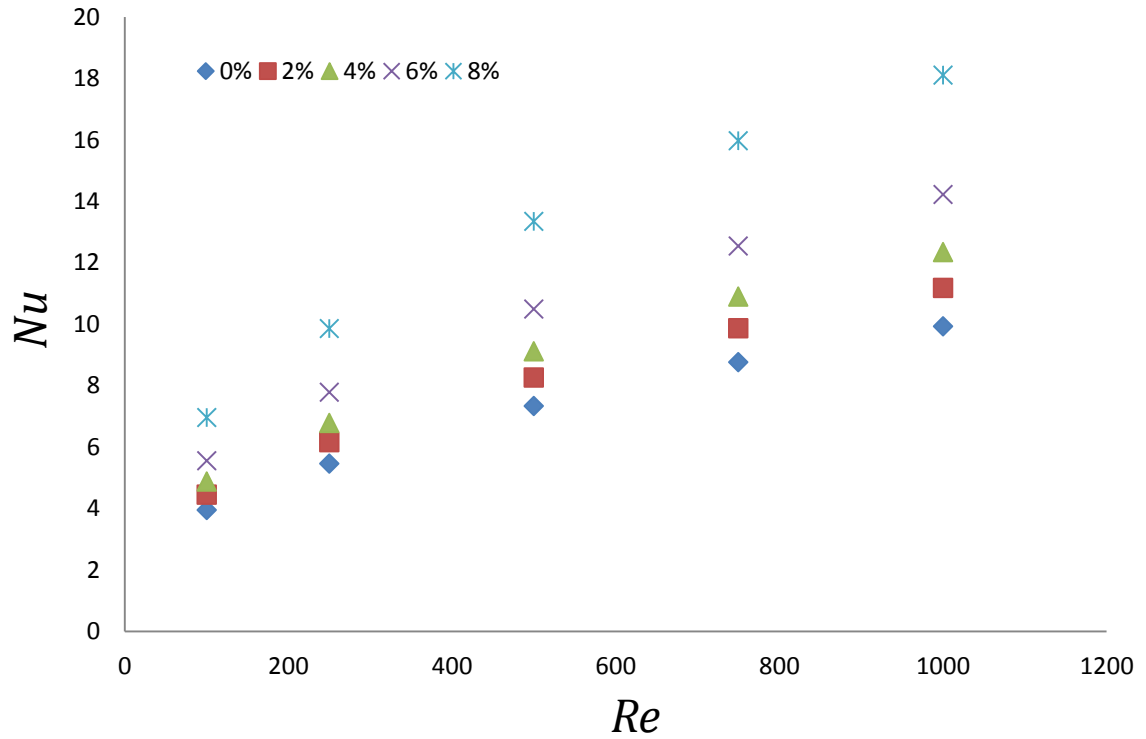


Figure 4-8 : Average Nusselt number ratios in entire pipes.

Table 4-1 : Variations of inlet velocities (m/s) with Reynolds number and concentration.

	0%	2%	4%	6%	8%
<b>10</b>	0.001004008	0.001116870	0.001343709	0.001832989	0.003334364
<b>100</b>	0.010040080	0.011168700	0.013437091	0.018329894	0.033343644
<b>250</b>	0.025100200	0.027921750	0.033592726	0.045824736	0.083359109
<b>500</b>	0.050200401	0.055843501	0.067185453	0.091649472	0.166718219
<b>750</b>	0.075300601	0.083765251	0.100778179	0.137474208	0.250077328
<b>1000</b>	0.100400802	0.111687001	0.134370905	0.183298944	0.333436438

The pressure drop through the curve is depicted in Figure 4-9. The pressure drop increases dramatically with the increment of the Reynolds number. The increasing rate of the pressure drop at the concentration of 8% with respect to the concentration of 0 % appears nearly 15 times higher at all the Reynolds numbers. This value is considerably high in comparison with the increasing rate of the heat transfer. Consequently, the high pressure drop for the nanofluid should be given careful consideration in designing heat exchangers although

the nanofluid does not have the characteristics such as poor suspension stability, channel clogging and system abrasion and so on.

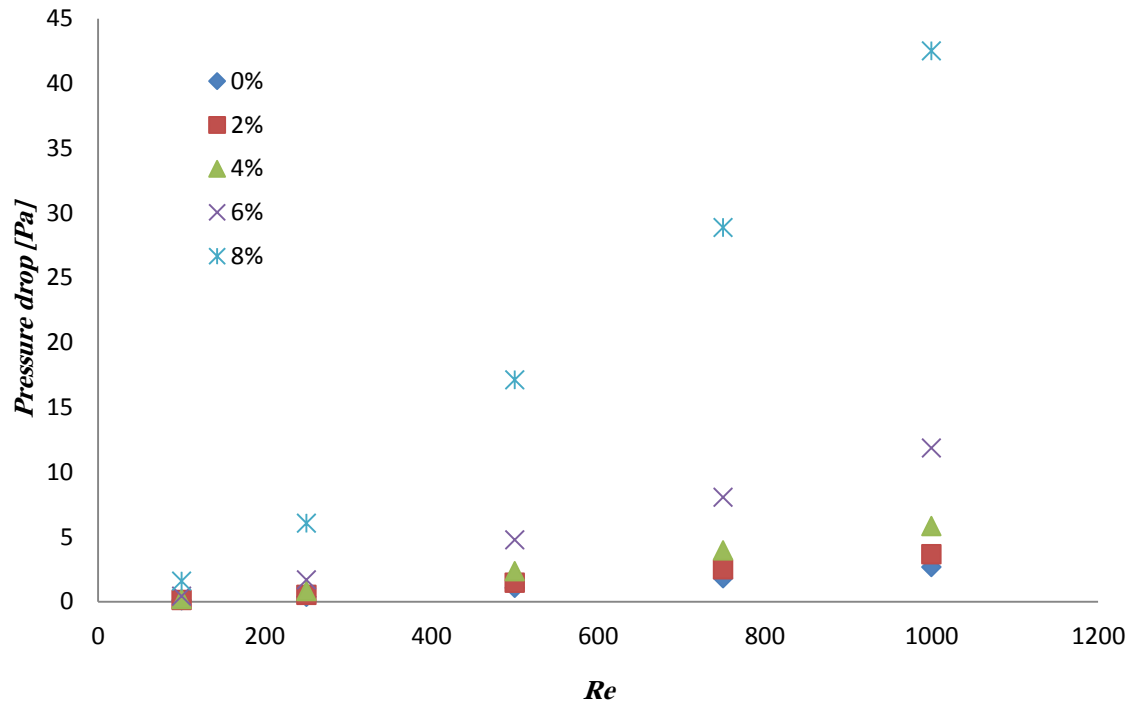


Figure 4-9 : Dependence of pressure drop on concentration at various Reynolds numbers.

The pressure drop with respect to the inlet velocity is illustrated in Figure 4-9. The pressure drop at the concentration of 8% is larger than that at the concentration of 0% because of the kinematic viscosity of the nanofluid.

# Chapter 5

## 5 CONCLUSION

The hydrodynamic and thermal analyses have been performed on the CUO-water nanofluid in the pipes with return bend. The results show that the suspended nanoparticles remarkably increase the heat transfer performance of the base fluid. From the results it was shown that as the volume fraction increases thermal conductivity ratio of the nanofluid will increase. This research also proved that with increase in volume fraction, the Nusselt number of the nanofluid will increase. This means that increased concentration of nanoparticles in the base fluid will increase the heat transfer performance of the nanofluid. For the same volume fraction, as the Reynolds number increases, the Nusselt number of the nanofluid increases. This shows that increase in flow rate of the nanofluid will increase the heat transfer performance of the nanofluid. Especially, the heat transfer enhancement in the return bend appears larger than that in the inlet and outlet pipes due to the effect of the secondary flow. However, the concentration increment of the nanofluid is accompanied by the high pressure drop in the pipe. Also, the increasing rate of the average Nusselt number is less than that of the thermal conductivity of the nanofluid with the augmentation of the concentration.

The increasing rate of the pressure drop in the nanofluid appears larger than the rate in the pure water. Meanwhile, the heat transfer characteristics of the nanofluid are improved with the increase of the specific heat.

## References

1. Vishwanadula, H., *Experimental investigations on the flow of nanofluids through circular pipes*. 2008: Southern Illinois University at Carbondale.
2. GHOBADIAN, R. and K. MOHAMMADI, Simulation of subcritical flow pattern in 180 uniform and convergent open-channel bends using SSIIM 3-D model. 2011. **4**(3).
3. Choi, S.U. and J. Eastman, *Enhancing thermal conductivity of fluids with nanoparticles*, 1995, Argonne National Lab., IL (United States).
4. Masuda, H., et al., Alteration of thermal conductivity and viscosity of liquid by dispersing ultra-fine particles. *Netsu Bussei*, 1993. **7**(2): p. 227-233.
5. Lee, S., et al., Measuring thermal conductivity of fluids containing oxide nanoparticles. *Journal of Heat Transfer*, 1999. **121**(2).
6. Wu, S., et al., Thermal energy storage behavior of Al<sub>2</sub>O<sub>3</sub>-H<sub>2</sub>O nanofluids. *Thermochimica Acta*, 2009. **483**(1): p. 73-77.
7. He, Y., et al., Numerical investigation into the convective heat transfer of TiO<sub>2</sub> nanofluids flowing through a straight tube under the laminar flow conditions. *Applied Thermal Engineering*, 2009. **29**(10): p. 1965-1972.
8. Prasher, R., et al., *Measurements of nanofluid viscosity and its implications for thermal applications*. *Applied Physics Letters*, 2006. **89**(13): p. 133108-133108-3.
9. Rajagopalan, R. and P.C. Hiemenz, *Principles of colloid and surface chemistry*. Principles of colloid and surface chemistry, 1997.
10. Fritsche, U.R., R.E.H. Sims, and A. Monti, *Direct and indirect land-use competition issues for energy crops and their sustainable production—an overview*. *Biofuels, Bioproducts and Biorefining*, 2010. **4**(6): p. 692-704.
11. Li, Q., *Investigation on Convective Heat Transfer and Flow Features of Nanofluids*. 2003.
12. Kulkarni, D.P., et al., Convective heat transfer and fluid dynamic characteristics of SiO<sub>2</sub> ethylene glycol/water nanofluid. *Heat Transfer Engineering*, 2008. **29**(12): p. 1027-1035.
13. Bergman, T.L., et al., *Fundamentals of heat and mass transfer*. 2011: Wiley.
14. Nguyen, C.T., et al., Heat transfer enhancement using Al<sub>2</sub>O<sub>3</sub>-water nanofluid for an electronic liquid cooling system. *Applied Thermal Engineering*, 2007. **27**(8): p. 1501-1506.
15. Duangthongsuk, W. and S. Wongwises, Heat transfer enhancement and pressure drop characteristics of TiO<sub>2</sub>-water nanofluid in a double-tube counter flow heat exchanger. *International Journal of Heat and Mass Transfer*, 2009. **52**(7): p. 2059-2067.
16. Kim, D., et al., Convective heat transfer characteristics of nanofluids under laminar and turbulent flow conditions. *Current Applied Physics*, 2009. **9**(2): p. e119-e123.
17. Abbasian, F., S. Yu, and J. Cao, Experimental and numerical investigations of three-dimensional turbulent flow of water surrounding a CANDU simulation fuel bundle structure inside a channel. *Nuclear Engineering and Design*, 2009. **239**(11): p. 2224-2235.
18. Corcione, M., M. Cianfrini, and A. Quintino, *Heat transfer of nanofluids in turbulent pipe flow*. *International Journal of Thermal Sciences*, 2012. **56**: p. 58-69.

19. Putnam, S.A., et al., *Thermal conductivity of nanoparticle suspensions*. Journal of Applied Physics, 2006. **99**(8): p. 084308-084308-6.
20. Venerus, D.C., et al., *Study of thermal transport in nanoparticle suspensions using forced Rayleigh scattering*. Journal of applied physics, 2006. **100**(9): p. 094310-094310-5.
21. Rusconi, R., E. Rodari, and R. Piazza, *Optical measurements of the thermal properties of nanofluids*. Applied physics letters, 2006. **89**(26): p. 261916-261916-3.
22. Maïga, S.E.B., et al., *Heat transfer enhancement by using nanofluids in forced convection flows*. International Journal of Heat and Fluid Flow, 2005. **26**(4): p. 530-546.
23. Zeinali Heris, S., M. Nasr Esfahany, and S.G. Etemad, *Experimental investigation of convective heat transfer of Al<sub>2</sub>O<sub>3</sub>/water nanofluid in circular tube*. International Journal of Heat and Fluid Flow, 2007. **28**(2): p. 203-210.
24. Behzadmehr, A., M. Saffar-Avval, and N. Galanis, *Prediction of turbulent forced convection of a nanofluid in a tube with uniform heat flux using a two phase approach*. International journal of heat and fluid flow, 2007. **28**(2): p. 211-219.
25. Pak, B.C. and Y.I. Cho, *Hydrodynamic and heat transfer study of dispersed fluids with submicron metallic oxide particles*. EXPERIMENTAL HEAT TRANSFER An International Journal, 1998. **11**(2): p. 151-170.
26. Xuan, Y. and Q. Li, *Investigation on convective heat transfer and flow features of nanofluids*. Journal of Heat Transfer, 2003. **125**: p. 151.
27. Buongiorno, J., *Convective transport in nanofluids*. Journal of Heat Transfer, 2006. **128**: p. 240.
28. Anderson, D.A., J.C. Tannehill, and R.H. Pletcher, *Computational fluid mechanics and heat transfer*. 1984.
29. Akin, J.E., *Finite elements for analysis and design*. 1994: Academic Pr.
30. Ramaswamy, B., *Finite element solution for advection and natural convection flows*. Computers & fluids, 1988. **16**(4): p. 349-388.
31. Ramaswamy, B., *Efficient finite element method for two-dimensional fluid flow and heat transfer problems*. Numerical Heat Transfer, 1990. **17**(2): p. 123-154.
32. Ramaswamy, B., T. Jue, and J. Akin, *Semi-implicit and explicit finite element schemes for coupled fluid/thermal problems*. International journal for numerical methods in engineering, 1992. **34**(2): p. 675-696.
33. Choi, J. and Y. Zhang, *Numerical simulation of laminar forced convection heat transfer of Al<sub>2</sub>O<sub>3</sub>-water nanofluid in a pipe with return bend*. International Journal of Thermal Sciences, 2012.
34. Akbarinia, A. and A. Behzadmehr, *Numerical study of laminar mixed convection of a nanofluid in horizontal curved tubes*. Applied Thermal Engineering, 2007. **27**(8): p. 1327-1337.
35. Maïga, S.E.B., et al., *Heat transfer behaviours of nanofluids in a uniformly heated tube*. Superlattices and Microstructures, 2004. **35**(3): p. 543-557.
36. Hamilton, R. and O. Crosser, *Thermal conductivity of heterogeneous two-component systems*. Industrial & Engineering chemistry fundamentals, 1962. **1**(3): p. 187-191.
37. Xuan, Y. and W. Roetzel, *Conceptions for heat transfer correlation of nanofluids*. International Journal of Heat and Mass Transfer, 2000. **43**(19): p. 3701-3707.

